Using redundant ancilla encoding and flags for very low overhead fault-tolerant magic state preparation

Christopher Chamberland[1, 2, *] and Kyungjoo Noh[3, †]

[1] *Amazon Web Services, Pasadena, CA, 91125, USA*
[2] *Institute for Quantum Information and Matter, California Institute of Technology, Pasadena, CA 91125, USA*
[3] *Department of Physics, Yale University, New Haven, CT, 06520, USA*

The overhead cost of performing universal fault-tolerant quantum computation for large scale quantum algorithms is very high. Despite several attempts at alternative schemes, magic state distillation remains one of the most efficient schemes for simulating non-Clifford gates in a fault-tolerant way. However, since magic state distillation circuits are not fault-tolerant, all Clifford operations must be encoded in a large distance code in order to have comparable failure rates with the magic states being distilled. In this work, we introduce a new concept which we call redundant ancilla encoding. The latter combined with flag qubits allows for circuits to both measure stabilizer generators of some code, while also being able to measure global operators to fault-tolerantly prepare magic states, all using nearest neighbor interactions. In particular, we apply such schemes to a planar architecture of the triangular color code family. In addition to our scheme being suitable for experimental implementations, we show that for physical error rates near 10^{-4} and under a full circuit level noise model, our scheme can produce magic states using an order of magnitude fewer qubits compared to the most competitive magic state distillation schemes. Further, we can take advantage of the fault-tolerance of our circuits to produce magic states with very low logical failure rates using encoded Clifford gates with noise rates comparable to the magic states being injected. Consequently, we believe our scheme to be suitable for implementing fault-tolerant universal quantum computation with hardware currently under development.

I. INTRODUCTION

In order to perform long quantum computations, universal fault-tolerant quantum computers will need to be built with the capability of implementing all gates from a universal gate set with very low logical error rates. Further, the overhead cost for achieving such low error rates will need to be low. Transversal gates are a natural way to implement fault-tolerant gates. Unfortunately, from the Eastin-Knill theorem, given any stabilizer code, there will always be at least one gate in a universal gate set that cannot be implemented using transversal operations at the logical level [1].

Several fault-tolerant methods for implementing gates in a universal gate set have been proposed [2–15]. Despite these various proposals, magic state distillation remains a leading candidate in the implementation of a universal fault-tolerant quantum computer [16–25]. Indeed, it had long been believed that implementing magic state distillation was the dominant cost of a universal fault-tolerant quantum computer. However, recent results have shown that this is not necessarily the case [26]. Despite the significant progress that has been made in reducing the cost of performing magic state distillation, the cost still remains high.

One of the reasons for the high costs of magic state distillation is that the Clifford circuits used to distill the magic states are often not fault-tolerant. Consequently, the Clifford gates must be encoded in some error correcting code (often the surface code) to ensure that these gates have negligible error rates compared to the magic states being injected. In [13], a fault-tolerant method for directly preparing $|H\rangle$-type magic states was proposed using the Steane code and flag-qubit circuits [27–36]. For physical error rates $p \gtrsim 10^{-5}$ and with idle qubits failing with error rates 100 times smaller than single-qubit gate error rates, it was shown that fewer qubits were required to prepare $|H\rangle$ states than the best known distillation schemes. Unfortunately, the scheme requires a large amount of non-locality and is scaled by concatenating the Steane code with itself, making it difficult to implement in a scalable way with realistic quantum hardware.

The Steane code belongs to the family of two-dimensional color codes [6, 37–39], which are topological codes. In particular, two-dimensional color codes have the nice property that all logical Clifford gates can be implemented using transversal operations. In particular, for a color code with n data qubits, the logical Hadamard gate is simply given by $\overline{H} = H^{\otimes n}$. This features makes color codes particularly well suited for preparing $|H\rangle$-type magic states. Furthermore, recent work introduced a simple and efficient decoding algorithm for color codes [40]. Such a decoding scheme was then extended to triangular color codes with boundaries, and a new scalable and efficient decoder which incorporates information from flag qubits was devised, resulting in a competitive threshold of 0.2% under a full circuit-level depolarizing noise model [36].

In this work we introduce a new fault-tolerant scheme to directly prepare an $|H\rangle$-type magic state encoded in

* cchmber@amazon.com; chamber@caltech.edu
† noh827@gmail.com

the triangular color code family. We propose an architecture to prepare the $|H\rangle$ state on a two-dimensional planar layout using only nearest neighbor interactions. The preparation scheme is fault-tolerant and achieves full code distance. Such an architecture was made possible not only with flag qubits, but also with a new technique which we call redundant ancilla encoding. In particular, a redundant amount of ancillas are used to measure the color code stabilizers, which turn into flag qubits when fault-tolerantly preparing a GHZ state for measuring the global operator $H^{\otimes n}$. We stress that such a scheme allows one to perform both stabilizer measurements and also measure global operators in a fault-tolerant way without having to change qubit layout.

Due to the fault-tolerance of our proposed architecture, magic states with very low logical error rates can be prepared without the need to use very large distance color codes or surface codes to encode the required Clifford operations. Indeed, we find that the encoded Clifford gates can have logical error rates comparable to the magic states being injected, thus significantly reducing the resource requirements to prepare very high fidelity magic states.

For physical error rates $p \gtrsim 10^{-4}$ and under a full circuit-level depolarizing noise model, we show that our scheme can be used to prepare magic states with logical error rates comparable to the best known magic state distillation protocols, but with at least an order of magnitude fewer qubits. For instance, to produce a magic state with a logical error rate of approximately 5×10^{-8}, our scheme requires only 64 qubits and all Clifford gate operations can be performed at the physical level. Since the magic states can be prepared on a two-dimensional architecture with nearest-neighbor interactions, we believe that our scheme is particularly well suited for quantum hardware currently under development.

The remainder of the manuscript is structured as follows. In Section II we provide the necessary background information relating to magic states and to the triangular color code family. In Section III we describe our fault-tolerant magic state preparation protocol using physical Clifford operations. In Section IV we provide the necessary details for computing the resource overhead requirements for our magic state preparation scheme and provide detailed numerical results. In Section V, we described how our scheme can be used with encoded stabilizer operations, and we provide numerical results for preparing $|H\rangle$ states using such encoded operations. In Section VI we conclude and discuss directions for future work.

II. PRELIMINARY MATERIAL

In order to make this paper as self-contained as possible, in this section we present the basic preliminary material required to understand the fault-tolerant magic state preparation scheme presented in Section III. We first introduce $|H\rangle$-type magic states in Section II A, followed by the triangular color code family in Section II B which we use to implemented encoded $|H\rangle$ states.

A. $|H\rangle$-type magic states.

The n-qubit Clifford group is defined as

$$\mathcal{P}_n^{(2)} = \{U : \forall P \in \mathcal{P}_n^{(1)}, UPU^\dagger \in \mathcal{P}_n^{(1)}\}, \tag{1}$$

where $\mathcal{P}_n^{(1)}$ is the n-qubit Pauli group. The Clifford group is generated by

$$\mathcal{P}_n^{(2)} = \langle H, Y\left(\frac{\pi}{2}\right), \text{CNOT}\rangle, \tag{2}$$

where

$$H = \frac{1}{\sqrt{2}}\begin{pmatrix} 1 & 1 \\ 1 & -1 \end{pmatrix}, \quad \text{and} \quad Y\left(\frac{\pi}{2}\right) = \frac{1}{\sqrt{2}}\begin{pmatrix} 1 & -1 \\ 1 & 1 \end{pmatrix}. \tag{3}$$

Here H is the Hadamard gate, $Y\left(\frac{\pi}{2}\right) = e^{-i\frac{\pi}{4}Y}$ and the CNOT gates acts as

$$\text{CNOT}|a\rangle \otimes |b\rangle = |a\rangle \otimes |a \oplus b\rangle, \tag{4}$$

on the computational basis states $|a\rangle$ and $|b\rangle$. The Clifford group, along with the non-Clifford gate[1]

$$T = e^{-i\frac{\pi Y}{8}} = \begin{pmatrix} \cos\frac{\pi}{8} & -\sin\frac{\pi}{8} \\ \sin\frac{\pi}{8} & \cos\frac{\pi}{8} \end{pmatrix}, \tag{5}$$

forms a universal gate set (note that $T = \text{diag}(1, e^{i\pi/4})$ is Clifford equivalent to the T gate defined in Eq. (5)). Hence defining $\mathcal{G} = \langle H, Y\left(\frac{\pi}{2}\right), T, \text{CNOT}\rangle$, and given a target fidelity ϵ, a unitary operator U can be approximated with $\mathcal{O}(\log^c 1/\epsilon)$ gates in $\mathcal{G}$ [41, 42].

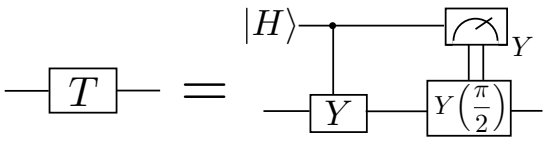

FIG. 1. Circuit for simulating a T gate using one copy of an $|H\rangle$ state and stabilizer operations. If the Y-basis measurement outcome is $+1$, a $Y\left(\frac{\pi}{2}\right)$ gate is applied to the data qubit, otherwise $Y\left(\frac{\pi}{2}\right)$ is not applied.

A magic state is a state that can be used as a resource state to simulate non-Clifford gates using only stabilizer

[1] Unless otherwise specified, whenever we refer to T gates throughout this paper, they will always correspond to the gate given in Eq. (5).

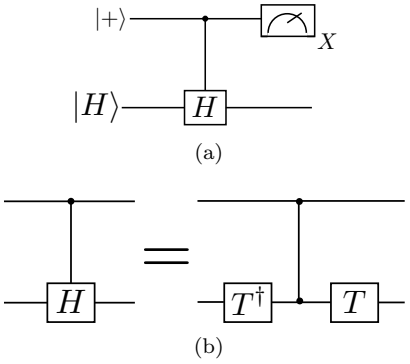

FIG. 2. (a) Circuit used to implement a non-destructive measurement of the Hadamard operator. (b) Decomposition of the controlled Hadamard gate in terms of T and $T^\dagger$ gates and a controlled-Z gate (which belongs to $\mathcal{P}_n^{(2)}$).

operations (i.e. Clifford gates, computational basis states and Z-basis measurements). Additionally, magic states can also be distilled using only stabilizer operations [16]. In this paper we focus entirely on preparing an $|H\rangle$-type magic state [16, 18]. In particular, an $|H\rangle$ state is given by

$$|H\rangle = \cos\frac{\pi}{8}|0\rangle + \sin\frac{\pi}{8}|1\rangle = T|0\rangle, \tag{6}$$

which is a $+1$ eigenstate of H. Note that $|H\rangle$ is Clifford equivalent to the state

$$|A_{\frac{\pi}{4}}\rangle \equiv \frac{1}{\sqrt{2}}(|0\rangle + e^{i\frac{\pi}{4}}|1\rangle) = e^{i\frac{\pi}{8}}HS^\dagger|H\rangle, \tag{7}$$

where $S = \mathrm{diag}(1, i)$ is the phase gate. The state $|A_{\frac{\pi}{4}}\rangle$ can be used to simulate the $T = \mathrm{diag}(1, e^{i\pi/4})$ gate using stabilizer operations.

In Fig. 1, we provide the circuit used to simulate the T gate in Eq. (5) using one $|H\rangle$ state in addition to stabilizer operations. In many physical implementations, noisy $|H\rangle$ states are injected into such circuits. To determine if an $|H\rangle$ state is afflicted by an error, one can measure the Hadamard operator using the circuit show in Fig. 2a. Since $HY|H\rangle = -Y|H\rangle$, if $|H\rangle$ is afflicted by a Y error, a -1 measurement outcome will be obtained. Further, if $|H\rangle$ is afflicted by an X or Z error, then the measurement outcome are ± 1 at random. If the outcome is $+1$, then no error will be present after the measurement. Note that the controlled-Hadamard gate can be decomposed into products of T, $T^\dagger$ and controlled-Z gates as shown in Fig. 2b.

The goal of this work is to produce encoded $|H\rangle$ states with very low logical failure rates using the fewest possible resources along with an architecture which is suitable for realistic hardware implementations. Along with fault-tolerant implementations of logical Clifford gates, such encoded $|H\rangle$ states could then be used for universal fault-tolerant quantum computation with very low overhead to implement quantum algorithms on near term quantum hardware.

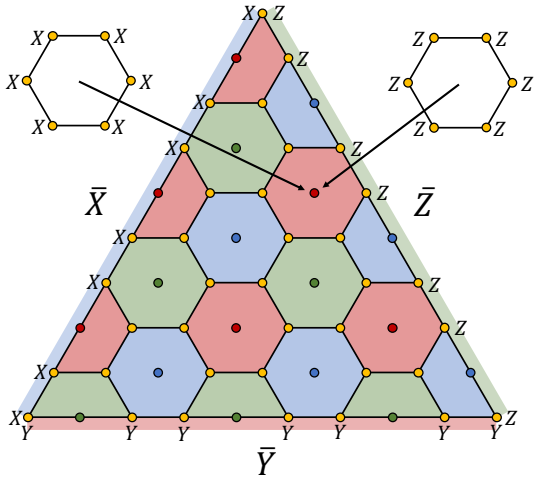

FIG. 3. Lattice $\mathcal{L}$ for the implementation of the triangular color code (in this case a distance $d = 5$ color code). Each face of $\mathcal{L}$ consists of both X and Z-type stabilizer generators which are supported on all qubits belonging to the face. The logical X and Z operators are given by tensor products of all X and all Z operators along a boundary of the triangle.

B. Triangular color code family

Color codes are topological codes, and thus the data qubits can placed on a lattice where each stabilizer generator can be measured using nearest neighbor interactions. The triangular color code family has code parameters $[\![n = (3d^2+1)/4, 1, d]\!]$ and is a version of the color code defined on a two-dimensional lattice $\mathcal{L}$ with boundaries. It is a self-dual CSS code with weight-four and weight-six X and Z-type stabilizers (see Fig. 3). The lattice $\mathcal{L}$ is 3-colorable, meaning that every face can be colored in red, green or blue with any other face sharing an incident edge having a different color. All vertices of $\mathcal{L}$ (apart from the three corners) are incident to three edges. Further, triangular color codes can implement all logical Clifford gates using transversal operations. In particular, the logical Hadamard operator is simply given by $\overline{H} = H^{\otimes n}$ where n is the number of data qubits.

In [40], an efficient decoder (which we refer to as the `Lift` decoder) for two-dimensional color codes was provided. In [36] it was shown how the `Lift` decoder can be extended to color codes with boundaries. Further, it was shown how the `Lift` decoder can incorporate measurement outcomes from flag qubits to maintain the effective distance of the code under a full circuit level noise model (see below). Using such methods, it was found that triangular color codes exhibit a competitive threshold value of 0.2% under a full circuit-level depolarizing noise model.

It is clear from Section II A that the logical Hadamard operator can be measured by applying a controlled Hadamard gate between ancillas and every data qubit

of a triangular color code. In Section III, we focus on providing an architecture for triangular color codes allowing the logical Hadamard operator to be measured in a fault-tolerant way using only nearest neighbor interactions. We then show how an encoded $|H\rangle$-type magic state can be fault-tolerantly prepared with very low qubit overhead.

In what follows, the full circuit level noise model used throughout all simulations performed in this work with physical stabilizer operations is given as follows:

1. With probability p, each single-qubit gate location is followed by a Pauli error drawn uniformly and independently from $\{X, Y, Z\}$.

2. With probability p, each two-qubit gate is followed by a two-qubit Pauli error drawn uniformly and independently from $\{I, X, Y, Z\}^{\otimes 2} \setminus \{I \otimes I\}$.

3. With probability $\frac{2p}{3}$, the preparation of the $|0\rangle$ state is replaced by $|1\rangle = X|0\rangle$. Similarly, with probability $\frac{2p}{3}$, the preparation of the $|+\rangle$ state is replaced by $|-\rangle = Z|+\rangle$.

4. With probability p, the preparation of the $|H\rangle$ state is replaced by $P|H\rangle$ where P is a Pauli error drawn uniformly and independently from $\{X, Y, Z\}$.

5. With probability $\frac{2p}{3}$, any single qubit measurement has its outcome flipped.

6. With probability p, each idle gate location is followed by a Pauli error drawn uniformly and independently from $\{X, Y, Z\}$.

III. FAULT-TOLERANT $|H\rangle$ STATE PREPARATION SCHEME

In order for an $|H\rangle$-type magic state to be useful for performing long quantum computations, it is important to be able to prepare such states with very high fidelity. Depending on size and duration of a quantum algorithm, the desired probability that an $|H\rangle$ state is afflicted by an error ranges from 10^{-7} to 10^{-15} [43–45]. Efficient magic state distillation protocols have been devised to prepare such states encoded in an error correcting code with very low error rates [19, 22–26, 45]. However, as mentioned in Section I, magic state distillation circuits are typically not fault-tolerant. Therefore, under a full circuit level noise model (and since two qubit gates are often the noisiest component of a quantum device), each Clifford operation must be encoded in some large error correcting code in order for Clifford gate errors to be negligible.

We now present a fault-tolerant method for preparing an $|\overline{H}\rangle$ state encoded in a triangular color code using only nearest neighbor interactions[2]. Such methods makes use of flag qubits, in addition to a technique which we refer to as redundant ancilla encoding. Since our scheme is fault-tolerant, it will be shown that high fidelity magic states can be obtained using physical Clifford operations in the presence of the full circuit-level depolarizing noise model described in Section II B. For even higher fidelity magic states, we will show that when applying our scheme with logical Clifford operations, such gates can have failure rates which are commensurate with the injected magic states used to implemented T gates (see Figs. 1 and 2b). Hence only small to intermediate sized codes will be necessary to encode the Clifford operations.

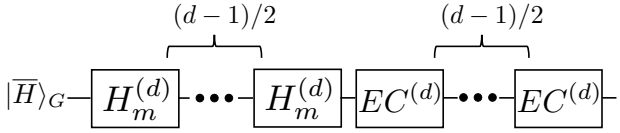

FIG. 4. General scheme for the fault-tolerant preparation of an encoded magic state $|\overline{H}\rangle$. First, a physical $|H\rangle$ state is grown to an encoded $|\overline{H}\rangle$ state of a distance d trianguluar color code (represented by the label $|\overline{H}\rangle_G$). Second, a t-flag circuit (with $t = (d-1)/2$) for performing a non-destructive measurement of $\overline{H}$ (labelled as $H_m^{(d)}$) is applied $(d-1)/2$ times. In particular, for each round, a GHZ ancilla is constructed in a fault-tolerant way to measure $H^{\otimes n}$. Third, $(d-1)/2$ rounds of error correction for the distance d triangular color code (each labelled $EC^{(d)}$) are applied to the encoded $|\overline{H}\rangle$ state. If any flag qubits flag, or the ancilla measurements in either $H_m^{(d)}$ or $EC^{(d)}$ are non-trivial, the protocol is aborted.

Flag qubits are ancilla qubits used to detect and identify high weight errors arising from a small number of faults between gates which entangle the encoded data with ancillary systems used to perform the necessary measurements for error correction [28, 30]. When the measurement outcome of a flag qubit is non-trivial (i.e. -1 instead of $+1$), we say that the flag qubit flagged. We now provide an important definition which is an extension of a definition first introduced in [30]:

Definition 1. *t-flag circuit*
A circuit $C(\overline{U})$ which, when fault-free, implements a projective measurement of a weight-w operator $U \in \mathcal{P}_n^{(2)}$ without flagging is a t-flag circuit if the following holds: For any set of v faults at up to t locations in $C(U)$ resulting in an error E with $min(wt(E), wt(EU)) > v$, the circuit flags.

In other words, a t-flag circuit guarantees that at least one flag qubit flags whenever there are $v \leq t$ faults resulting in a data qubit error of weight greater than v.

When growing a physical $|H\rangle$ state into an encoded $|\overline{H}\rangle$ of a distance d triangular color code, $v < (d-1)/2$ faults

[2] In what follows, a bar above the $|H\rangle$ symbol always correspond to an encoded $|H\rangle$ state.

can result in an output state of the form $E'\overline{E}|\overline{H}\rangle$ where E' is a detectable error by the color code (i.e. $s(E') \neq \mathbf{0}$ where $s(E)$ is the error syndrome of E) and $\overline{E}$ is a logical error of the color code. The preparation of $|\overline{H}\rangle$ can be made fault-tolerant by performing an encoded version of the non-destructive Hadamard measurement (the circuit in Fig. 2a) to detect $\overline{E}$ followed by rounds of error correction (EC) to detect the error E' [13, 46]. The underlying scheme that we use to perform such operations is illustrated in Fig. 4. The scheme consists of three parts. In the first step, we grow a physical $|H\rangle$ state to an encoded $|\overline{H}\rangle$ state, which we label as $|\overline{H}\rangle_G$. Next, we use $(t = (d-1)/2)$-flag circuits to perform a non-destructive measurement of $\overline{H}$ (labelled as $H_m^{(d)}$). In particular, a GHZ state is constructed in such a way that the $H^{\otimes n}$ measurement is fault-tolerant. Lastly, error correction is performed to detect the errors E' using $t = (d-1)/2$-flag circuits (labelled $EC^{(d)}$). If any of the flag qubits flag, or the parity of any ancilla measurements in the circuits $H_m^{(d)}$ or $EC^{(d)}$ is odd, the protocol is aborted and starts anew.

As shown in Appendix B, both the $H_m^{(d)}$ and $EC^{(d)}$ circuits need to be repeated $(d-1)/2$ times to guarantee the fault-tolerance of our scheme. Further, the circuits used for the $H_m^{(d)}$ and $EC^{(d)}$ operations need to be $t = (d-1)/2$-flag circuits to prevent errors from spreading to uncorrectable errors. In Sections III B and III C, such circuits are provided using only nearest neighbor interactions for $d \in \{3, 5, 7\}$. A key idea which allows us to use the same two-dimensional qubit layout and nearest-neighbor interactions to perform **both** the non-destructive Hadamard measurement and the stabilizer measurements of the triangular color code is the use of redundant ancilla encoding and flag qubits (see Section III B).

Note that although our scheme applies for code distances $d \leq 7$, in Section IV we show that encoded $|\overline{H}\rangle$ states can be prepared with similar logical failure rates but with orders of magnitude fewer qubits (for physical error rates $p \gtrsim 10^{-4}$) compared to some of the state of the art magic state distillation schemes (such as those in [26]).

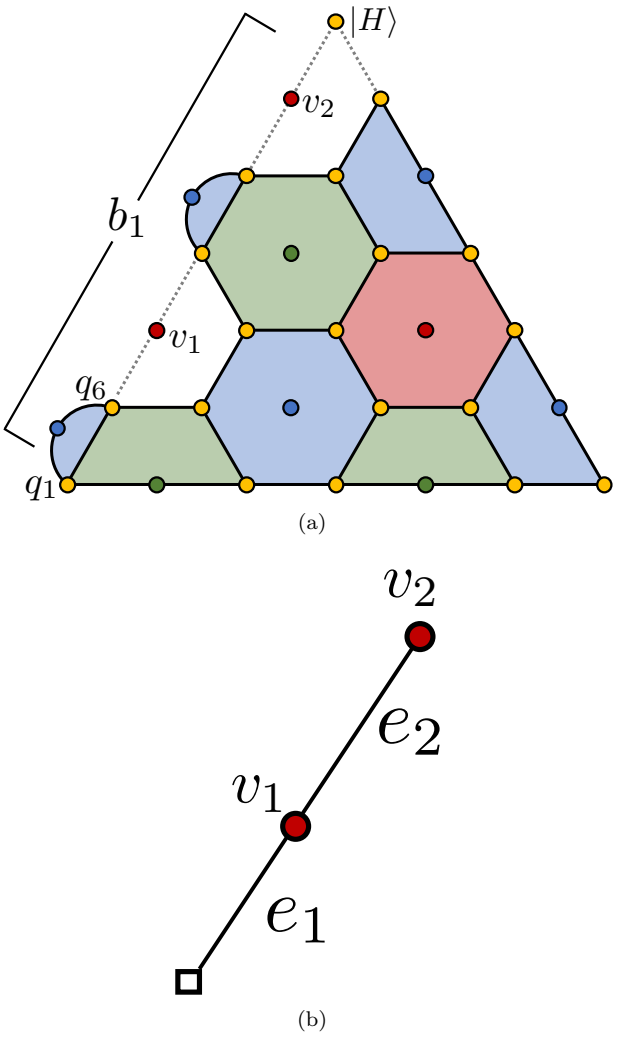

FIG. 5. (a) Growing a physical $|H\rangle$ state to a distance $d = 5$ color code. First, a stabilizer state $|S_t\rangle$ is prepared with stabilizers given by the red, green and blue plaquettes. The encoded $|\overline{H}\rangle$ state is then obtained by measuring both weight-four X followed by Z-type operators (represented by white plaquettes) along the boundary of the triangle. Such measurements are random since the weight-four operators don't commute with the weight-two stabilizers of $|S_t\rangle$. (b) Matching graph ($G_{1x}^{(5)}$ and $G_{1z}^{(5)}$) used to implement weight-two corrections arising from -1 measurement outcomes for generators of $\mathcal{S}_{b_1}$. As an example, if the vertex v_1 is highlighted, after implementing MWPM, the edge e_1 would be selected resulting in the correction $Z_{q_1}Z_{q_6}$.

A. Growing a physical $|H\rangle$ state to an encoded $|\overline{H}\rangle$ state in a distance d triangular color code ($|\overline{H}\rangle_G$)

An illustration for growing a physical $|H\rangle$ state to an encoded $d = 5$ $|\overline{H}\rangle$ state is given in Fig. 5a. The preparation of $|\overline{H}\rangle$ in a general distance d triangular color code can be done as follows. First, one prepares a stabilizer state $|S_t\rangle$ (which encodes no logical qubits) that is stabilized by all elements in $\mathcal{S}_{\text{st}} = \mathcal{S}_{w_2} \cup (\mathcal{S}_{\text{color}} \setminus \mathcal{S}_{b_1})$ where $\mathcal{S}_{\text{color}}$ is the stabilizer group of a distance d triangular color code, $\mathcal{S}_{b_1}$ is generated by the X and Z-type weight-four operators (white plaquettes) along the boundary b_1 of the triangular color code and $\mathcal{S}_{w_2}$ is generated by the weight-two X and Z-type operators along the boundary b_1 (see Fig. 5a for the case where $d = 5$). The qubit which is in the support of $\text{supp}(\mathcal{S}_{\text{color}}) \setminus \text{supp}(\mathcal{S}_{\text{st}})$ is prepared in the $|H\rangle$ state. Note that in the above construction, any of the three boundaries of $\mathcal{L}$ can be chosen. We chose b_1 for convention.

After preparing $|S_t\rangle$, the X and Z-type generators of $\mathcal{S}_{b_1}$ are measured along the boundary b_1. Since the generators of $\mathcal{S}_{b_1}$ don't commute with with the weight-two generators of $\mathcal{S}_{w_2}$, the measurement outcomes of each

generator in $\mathcal{S}_{b_1}$ will be ± 1 at random. If a -1 outcome is obtained, a Pauli frame update [47–50] needs to be applied to obtain the correct encoded state. In order to perform the correct Pauli frame update based on the random measurement outcomes, we define two one-dimensional graphs $G^{(d)}_{1x}$ and $G^{(d)}_{1z}$. The vertices of the graph $G^{(d)}_{1x}$ contain the random measurement outcomes of the X-type generators in $\mathcal{S}_{b_1}$. Each edge corresponds to two qubits which have support one of the weight-two operators of $\mathcal{S}_{w_2}$. Similarly, the vertices of the graph $G^{(d)}_{1z}$ encodes the random measurement outcomes of the Z-type generators in $\mathcal{S}_{b_1}$. An example is provided in Fig. 5b for the $d = 5$ triangular color code. Given the set of highlighted vertices of $G^{(d)}_{1x}$ and $G^{(d)}_{1z}$, Minimum-Weight-Perfect-Matching (MWPM) [51] is applied on both graphs. Each highlighted edge involves performing a weight-two X or Z-type Pauli frame update. For instance, for the graph $G^{(5)}_{1x}$ in Fig. 5b, if the edge e_1 is selected during MWPM, the correction $Z_{q_1}Z_{q_6}$ is applied to the data. Note that the growing scheme is not fault-tolerant, and thus there is no need to repeat the measurements described above. More details on the implementation of $|\overline{H}\rangle_G$ are provided in Appendix A.

B. Performing error correction ($EC^{(d)}$) using redundant ancilla encoding

In this section we describe the error correction circuits ($EC^{(d)}$) used to detect errors at the output of the $H^{(d)}_m$ circuits. In particular, to guarantee fault-tolerance (see Definition 2 in Appendix B for our definition of fault-tolerance) of our scheme, we require that each $EC^{(d)}$ circuit is at least a one-flag circuit. For instance, if two faults in two separate Z-type stabilizers both result in a weight-two data qubit error without any flag qubits flagging, such an error might not be correctable by a $d = 5$ triangular color code. Hence such circuits certainly don't satisfy Definition 2. Note that in [36], it was proved that only one flag circuits are required when performing error correction with the triangular color code. The need for only one-flag circuits has to do with the fact that if two-faults occur during a weight-six stabilizer measurement resulting in a weight-three data qubit error, such an error cannot have full support along a minimum-weight logical operator of the triangular color code.

In Fig. 6a we illustrate the full $EC^{(5)}$ circuit used to measure the stabilizers of a triangular color code along with the CNOT gate scheduling which minimizes the circuit depth for the given qubit layout. The weight-four stabilizers are identical to the ones used in [36]. However, an important difference can be observed for the weight-six stabilizers, which in addition to using three flag qubits, also uses three ancilla qubits. If an error anti-commutes with a weight-six stabilizer, the measurement outcomes of the three ancillas will have odd parity, otherwise it will have even parity[3]. The circuit for measuring a weight-six X-type stabilizer which respects the CNOT scheduling is given in Fig. 6b. By performing an exhaustive numerical search, we verified that both weight-four and weight-six circuits are two-flag circuits. Since the weights of the stabilizer generators are independent of d, having two-flag circuits is sufficient to ensure that the $EC^{(d)}$ circuits are implemented fault-tolerantly [30]. Lastly, each weight-four and and weight-six plaquette in a general $EC^{(d)}$ circuit has the same qubit layout and gate connectivity as those of Fig. 6a.

Now, one might wonder why three ancilla qubits instead of a single ancilla are used for measuring the weight-six stabilizers (see for instance the weight-six circuits used in [36] which only uses one ancilla). Indeed if one is only interested in performing fault-tolerant error correction instead of fault-tolerant quantum computation, then a single ancilla qubit suffices, since the additional ancillas don't provide more information and also increase the circuit depth. However in Section III C, we show that to use the same qubit layout for measuring the operator $\overline{H} = H^{\otimes n}$ (which is a global operator), the roles of the ancillas and flags in Fig. 6a are reversed. In other words, the ancilla qubits become flag qubits and vice-versa. To ensure that the circuit $H^{(d)}_m$ is a $t = (d-1)/2$-flag circuit for $d \leq 7$, we require three flag qubits for every weight-six plaquette and one flag qubit for every weight-four plaquette. Hence if only a single ancilla qubit were used in Fig. 6b, the circuit $H^{(7)}_m$ would not be a three-flag circuit, which would significantly reduce the performance of our protocol (in fact, it would not be possible to achieve the full color code distance for $d > 5$).

To conclude this section, more ancilla qubits than necessary are used to measure the stabilizer generators of the triangular color code. However using the same qubit layout, the extra ancillas (which become flag qubits when measuring $H^{\otimes n}$) ensures that the circuit for measuring the global operator $H^{\otimes n}$ is a $t = (d-1)/2$-flag circuit so that at least $(d+1)/2$ faults are required to produce a logical failure for the scheme in Fig. 4. We refer to this extra redundancy as **redundant ancilla encoding**. In Section III C we provide explicit circuit constructions to measure $H^{\otimes n}$.

C. t-flag circuit construction for the non-destructive measurement of $\overline{H}$ ($H^{(d)}_m$)

Here, we describe in detail how to construct a t-flag circuit ($t = (d-1)/2$) for the non-destructive measurement of the logical Hadamard operator (i.e., $H^{(d)}_m$). The

[3] This is similar to error correction circuits used for Shor error correction [52, 53]. However an important difference is that ancilla verification (i.e. using several ancillas to measure pairs of qubits) is not necessary since the flag qubits ensure that the circuit in Fig. 6b is a two-flag circuit.

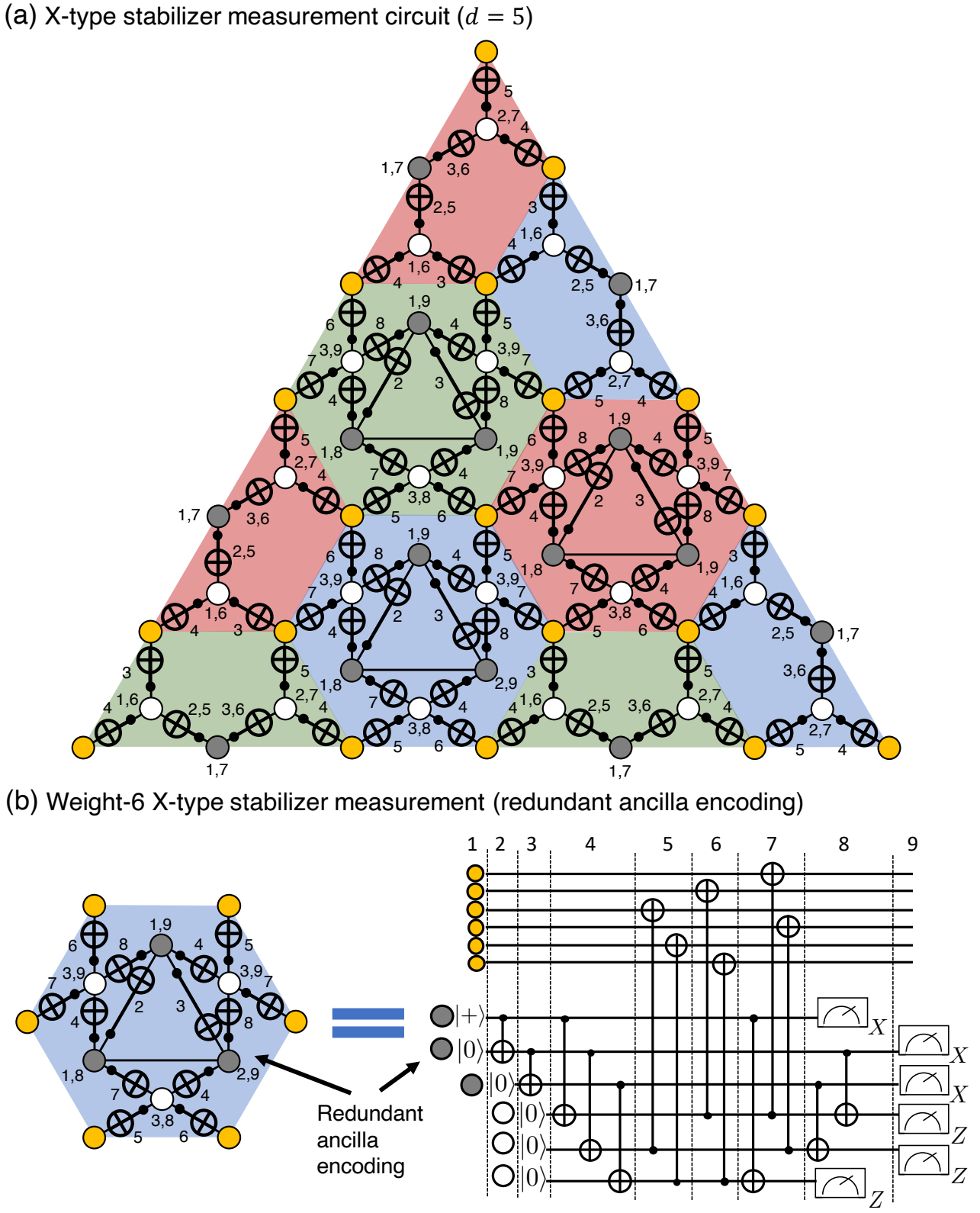

FIG. 6. (a) $EC^{(5)}$ circuit for detecting errors at the output of the $H_m^{(5)}$ circuit. The grey circles correspond to the ancilla qubits used to measure the parity of the stabilizers, whereas the white circle correspond to the flag qubits. The CNOT gate scheduling which minimizes the total number of time steps for measuring the X and Z-stabilizers is also provided. One round of X or Z-type stabilizer measurements requires a total of nine time steps. (b) Circuit for measuring a weight-six X stabilizer of the triangular color code. The grey circles correspond to the ancilla qubits and the white circles to the flag qubits.

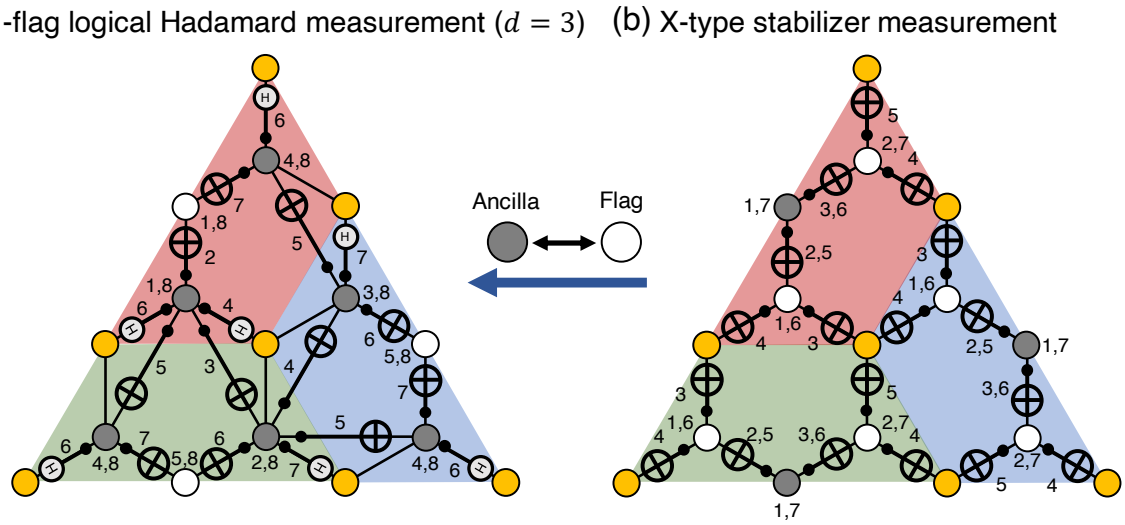

FIG. 7. (a) A 1-flag circuit $H_m^{(3)}$ for the measurement of the logical Hadamard operator $H^{\otimes 7}$ of the $d = 3$ triangular color code. (b) A circuit for the measurement of the X-type stabilizers of the $d = 3$ triangular color code. Note that there is a role reversal between the ancilla qubits (grey circles) and the flag qubits (white circles). That is, the ancilla (or flag) qubits in the stabilizer measurement circuit are used as flag (or ancilla) qubits in the Hadamard measurement circuit. Also, the controlled-H symbols in (a) represent the controlled-Hadamard gates.

circuits we construct apply to distance d color codes with $d \in \{3, 5, 7\}$. In Fig. 7a, we present a 1-flag circuit for the measurement of the logical Hadamard operator $H^{\otimes 7}$ of the $d = 3$ triangular color code. Note that we used the same qubit layout as in the case of the stabilizer measurement (shown in Fig. 7b) but there is a role reversal between the ancilla qubits (grey circles) and the flag qubits (white circles). That is, the ancilla qubits in the stabilizer measurement circuit are used as flag qubits in the logical Hadamard measurement circuit and vice versa.

We now explain why the circuit in Fig. 7a performs a non-destructive measurement of the logical Hadamard operator $H^{\otimes 7}$. Note that the ancilla qubits (grey circles) in Fig. 7a are prepared in the logical plus state of the 6-qubit repetition code (or the 6-qubit GHZ state $\frac{1}{\sqrt{2}}(|0\rangle^{\otimes 6} + |1\rangle^{\otimes 6})$ through the CNOT gates between the ancilla qubits (see Fig. 8a). Then, as shown in Fig. 8b, the 7 controlled-Hadamard gates implement a logical controlled-Hadamard gate between the ancilla 6-qubit repetition code and the data $d = 3$ color code. Eventually, the ancilla qubits (in the 6-qubit repetition code) are measured in the logical X basis via a $X^{\otimes 6}$ measurement (see Fig. 8d). Hence, the circuits in Figs. 8a, b, and d implement the simple non-destructive Hadamard measurement circuit in Fig. 2a, except that the ancilla qubits are now encoded in the 6-qubit repetition code and the data qubits are encoded in the triangular $d = 3$ color code.

The most important element of the logical Hadamard measurement circuit in Fig. 7 is the parity check of the ancilla GHZ state by using flag qubits (see Fig. 8c). Note that the flag qubits (white circles) non-destructively measure the parity of the ancilla GHZ state Z_1Z_2, Z_3Z_6, and Z_4Z_5, or the three stabilizers of the 6-qubit repetition code (we labeled the qubits from the top to the bottom and from the left to the right). These stabilizer measurements will be trivial if all the CNOT gates in Fig. 8a are perfect. However, there may be some non-trivial flag measurement outcomes if the CNOT gates can fail. In particular, there are several single CNOT gate failure events that can cause a data qubit error of weight-2 or higher. For the Hadamard circuit to be 1-flag, all these failure events should be caught by flag qubits. Indeed, we verify via a comprehensive numerical search that the logical Hadamard circuit in Fig. 7a is a 1-flag circuit by confirming that if there is a single fault at any location resulting in a data qubit error E with $\min(\mathrm{wt}(E), \mathrm{wt}(EH^{\otimes 7})) > 1$, at least one flag qubit flags.

Similarly, we construct a 2-flag circuit for the logical Hadamard measurement $H_m^{(d=5)}$ of the $d = 5$ triangular color code and 3-flag circuit $H_m^{(d=7)}$ for the $d = 7$ triangular color code (see Fig. 9). The design principle is essentially the same. That is, in the $d = 5$ case (i.e., $H_m^{(d=5)}$), we first generate a 21-qubit GHZ state in the ancilla qubits (grey circles), or equivalently, a logical plus state of the 21-qubit repetition code. The entangled ancilla qubits are then coupled to all the 19 data qubits (yellow circles) through controlled-Hadamard gates. Finally, the ancilla qubits (in the 21-qubit repetition code) are measured in the the logical X basis via a $X^{\otimes 21}$ measurement. Thus, the circuit in Fig. 9a implements a non-destructive measurement of the logical Hadamard mea-

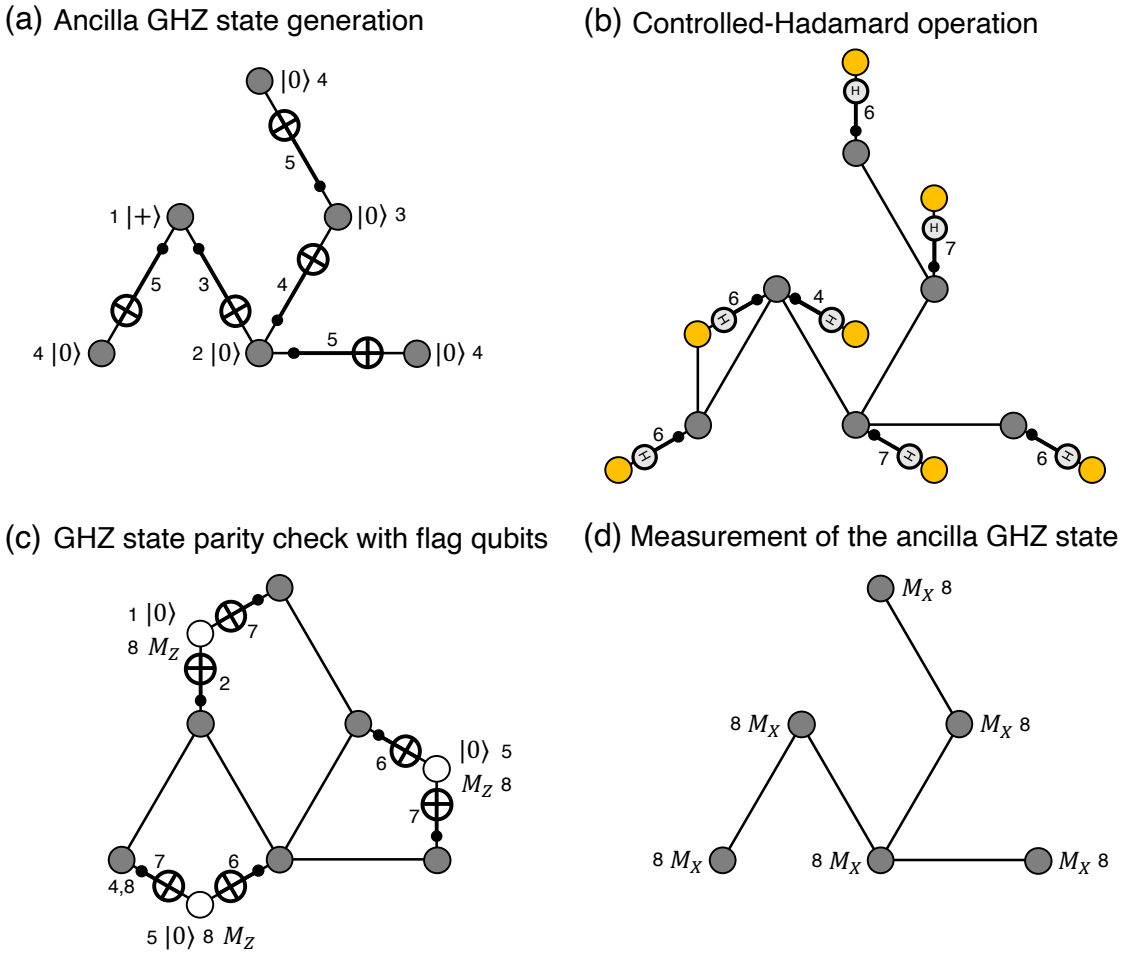

FIG. 8. The logical Hadamard circuit ($H_m^{(3)}$) in 7a can be decomposed into four elements, i.e., (a) preparation of the 6-qubit GHZ state $\frac{1}{\sqrt{2}}(|0\rangle^{\otimes 6} + |1\rangle^{\otimes 6})$ (or the logical plus state of the 6-qubit repetition code) in the ancilla qubits (grey circles), (b) controlled-Hadamard gates between the ancilla qubits (in the GHZ state) and the data qubits (yellow circles), (c) parity checks of the ancilla GHZ state by using flag qubits (white circles), and finally (d) measurement of the logical X operator $X^{\otimes 6}$ of the 6-qubit repetition code on the ancilla qubits.

surement of the $d = 5$ color code by using ancilla qubits in the 21-qubit repetition code.

Precisely because the ancilla qubits are encoded in the 21-qubit repetition code, we can check if the ancilla qubits are reliably prepared in the logical plus state by measuring 15 (out of 20) stabilizers of the ancilla 21-qubit repetition code using 15 flag qubits (white circles). We confirm via a comprehensive numerical search that the circuit $H_m^{(d=5)}$ is a 2-flag circuit. A 3-flag circuit for the logical Hadamard measurement $H_m^{(d=7)}$ of the $d = 7$ triangular color code is constructed in the same way by using 45 ancilla qubits prepared in the logical plus state of the 45-qubit repetition code, and using 36 flag qubits checking the 36 (out of 44) stabilizers of the 45-qubit repetition code (see Fig. 9b).

Recall that we used a redundant ancilla encoding scheme in the stabilizer measurement circuits (see Fig. 6). Specifically, we redundantly used three ancilla qubits to measure the weight-6 stabilizers of the triangular color code. Note that these ancilla qubits are used as flag qubits in the logical Hadamard measurement circuits $H_m^{(d)}$ with $d = 3, 5, 7$. Thus, the redundant ancilla encoding in the stabilizer measurement circuits allows the logical Hadamard measurement circuits to have sufficiently many flag qubits while maintaining the same two-dimensional qubit layout. In particular, the logical Hadamard measurement circuits $H_m^{(5)}$ and $H_m^{(7)}$ have 15 and 36 flag qubits that check 15 (out of 20) and 36 (out of 45) stabilizers of the ancilla GHZ state, respectively. Without the redundant ancilla encoding, we would have had 9 flag qubits in the $d = 5$ case and 18 flag qubits in the $d = 7$ case, as opposed to 15 and 36 flag qubits, respectively. We remark that the logical Hadamard measurement circuits $H_m'^{(5)}$ and $H_m'^{(7)}$ that are constructed with such fewer flag qubits are not 2-flag and 3-flag circuits. Thus, the redundant ancilla encoding scheme plays

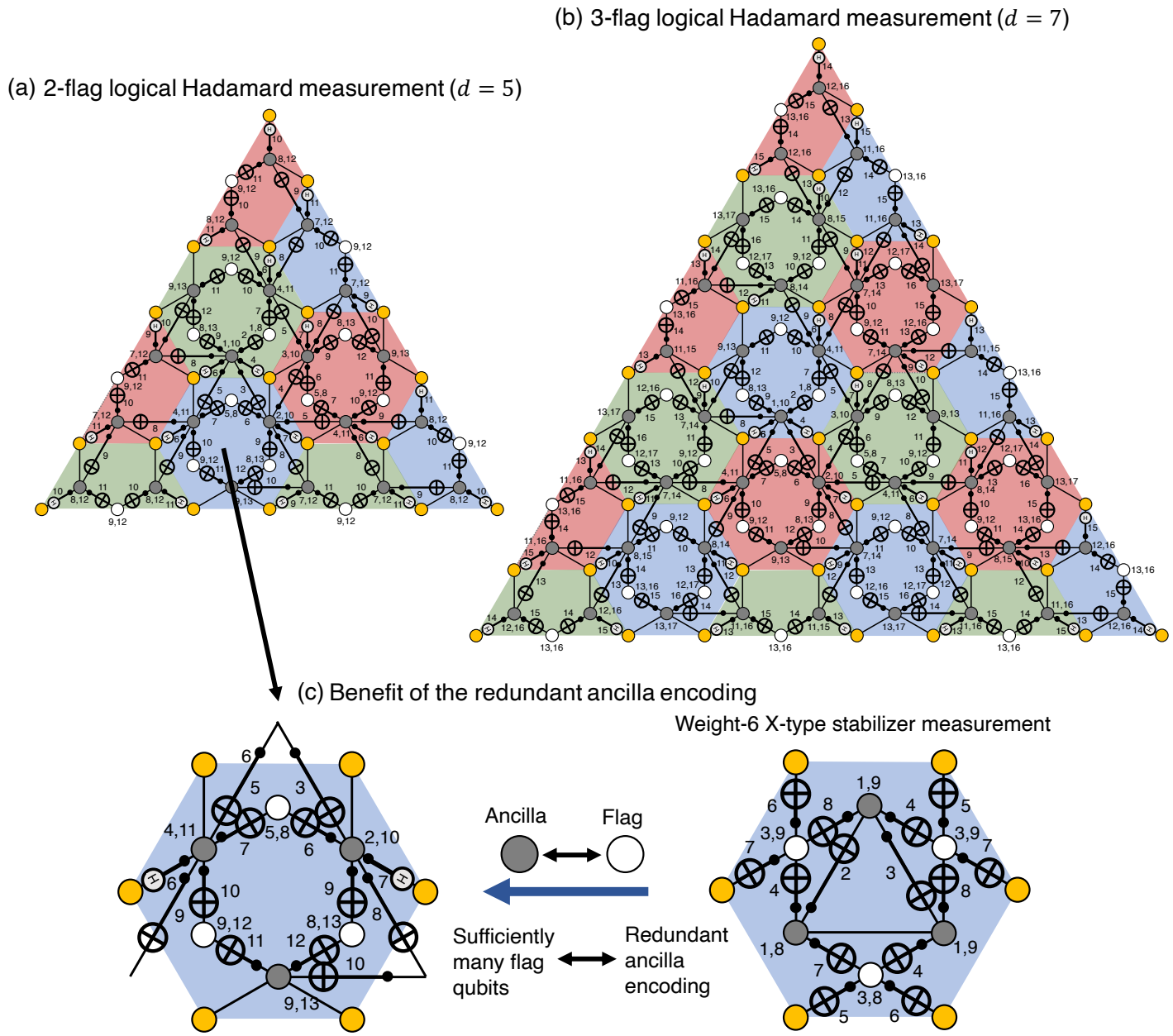

FIG. 9. (a) A 2-flag circuit $H_m^{(5)}$ for the measurement of the logical Hadamard operator $H^{\otimes 19}$ of the $d = 5$ triangular color code and (b) a 3-flag circuit $H_m^{(7)}$ for the measurement of the logical Hadamard operator $H^{\otimes 37}$ of the $d = 7$ triangular color code. (c) Illustration of the benefit of using redundant ancilla encoding. Note that the ancilla qubits in the stabilizer measurement circuits are used as flag qubits in the logical Hadamard measurement circuits. Thus, the redundant ancilla encoding in the stabilizer measurement circuits allows the logical Hadamard measurement circuits to have sufficiently many flag qubits.

a crucial role in guaranteeing the desired fault-tolerance property of the logical Hadamard measurement circuits.

IV. RESOURCE OVERHEAD FOR PREPARING ENCODED $|\overline{H}\rangle$ STATES WITH PHYSICAL CLIFFORD GATES

In this section we provide the logical failure rates of the states $|\overline{H}\rangle$ prepared using the scheme presented in Section III and the noise model described in Section II B. We also provide the average number of qubits required to produce such states.

$\lvert\overline{H}\rangle$ (physical Clifford's)	p	$p_L^{(d)}$	Average number of qubits
$d=3$	10^{-4}	3.45×10^{-6}	17
$d=5$	10^{-4}	3.6×10^{-8}	68
$d=7$	10^{-4}	4.9×10^{-10}	231
$d=3$	2×10^{-4}	1.39×10^{-5}	17
$d=5$	2×10^{-4}	3.01×10^{-7}	84
$d=7$	2×10^{-4}	7.83×10^{-9}	449
$d=3$	3×10^{-4}	3.11×10^{-5}	18
$d=5$	3×10^{-4}	1.10×10^{-6}	103
$d=7$	3×10^{-4}	3.97×10^{-8}	870
$d=3$	4×10^{-4}	5.64×10^{-5}	18
$d=5$	4×10^{-4}	2.48×10^{-6}	127
$d=7$	4×10^{-4}	1.25×10^{-7}	1,700
$d=3$	5×10^{-4}	8.51×10^{-5}	19
$d=5$	5×10^{-4}	5.23×10^{-6}	156
$d=7$	5×10^{-4}	3.06×10^{-7}	3,312

TABLE I. Logical error rate p_L and the average number of qubits $\langle n_{\rm tot}^{(d)}\rangle$ (see Eqs. (8) and (12)) of the $|\overline{H}\rangle$ state preparation scheme of Section III obtained from 10^9 Monte-Carlo simulations using the noise model of Section II B and simulation methods described in Section IV. For $p=10^{-4}$, only 68 and 231 qubits are required to prepare $|\overline{H}\rangle$ states with $p_L=3.6\times10^{-8}$ and $p_L=4.9\times10^{-10}$ respectively.

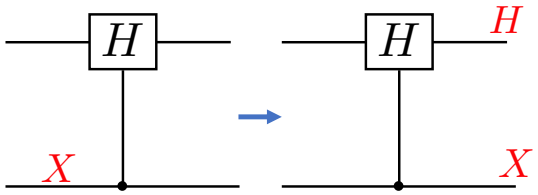

FIG. 10. An X error on the control qubit of the controlled-Hadamard gate results in an H error on the target qubit.

Since the whole sequence of operations in Fig. 4 fault-tolerantly prepares $|\overline{H}\rangle$ for $d\leq 7$, for a physical error rate p (see the description of the circuit-level noise model used in Section II B), the output state is afflicted by a logical fault with probability

$$p_L^{(d)}=\alpha p^{(d+1)/2}+\mathcal{O}(p^{(d+3)/2}), \tag{8}$$

where α counts all the combinations of $(d-1)/2$ faults which lead to acceptance of our scheme while resulting in a logical $\overline{X}$, $\overline{Y}$ or $\overline{Z}$ error. Hence

$$\alpha\leq\sum_{k=0}^{N}\binom{N}{\frac{d-1}{2}+k}, \tag{9}$$

where N is the total number of locations which can fail in the combined circuits of Fig. 4. For values of $p\leq10^{-3}$, the higher order terms in Eq. (8) were found to have a negligible impact on p_L.

Given the acceptance probability $p_{\rm acc}^{(d)}(p)$ for preparing a distance d encoded state $|\overline{H}\rangle$ with physical error rate p, the average number of qubits is given by

$$\langle n_{\rm tot}^{(d)}(p)\rangle=\frac{n^{(d)}+n_{\rm anc}^{(d)}}{p_{\rm acc}^{(d)}(p)}, \tag{10}$$

where $n^{(d)}=(3d^2+1)/4$ is the number of data qubits, and $n_{\rm anc}^{(d)}$ is the total number of ancilla and flag qubits used in the circuits $H_m^{(d)}$ and $EC^{(d)}$. Since each weight-six stabilizer generator requires six qubits, and each weight-four stabilizer three qubits, we have

$$n_{\rm anc}^{(d)}=6n_{w6}^{(d)}+3n_{w4}^{(d)}, \tag{11}$$

where $n_{w4}^{(d)}=(3/2)(d-1)$ and $n_{w6}^{(d)}=(3d^2-12d+9)/8$ are the number of weight-four and weight-six stabilizers. Putting everything together, we obtain

$$\langle n_{\rm tot}^{(d)}\rangle=\frac{6d^2-9d+5}{2p_{\rm acc}^{(d)}(p)}. \tag{12}$$

It is important to point out that due to the presence of T gates (which are non-Clifford) used to implement the controlled-Hadamard gates (see Fig. 2b), an efficient Monte-Carlo simulation of the circuits $H_m^{(d)}$ using Gottesman-Knill error propagation [54, 55] is not possible. Consequently, we divided the Monte-Carlo simulation to calculate $p_L^{(d)}$ and $p_{\rm acc}^{(d)}(p)$ into two parts. First, we perform a Monte-Carlo simulation of the circuit used to prepare $|\overline{H}\rangle_G$. If the output error $E_{\rm out}$ has a non-trivial syndrome or is a logical operator, the protocol of Section III is aborted, otherwise, we proceed to simulate the $H_m^{(d)}$ and $EC^{(d)}$ circuits. We define $p_{{\rm acc},1}^{(d)}$ to be

the probability of proceeding to the $H_m^{(d)}$ and $EC^{(d)}$ circuits. Note that there could be other faults in the $H_m^{(d)}$ and $EC^{(d)}$ circuits that would cause the protocol to be accepted even though E_{out} had a non-trivial syndrome or was a logical operator. However such an event would require at least $(d-1)/2$ faults, and since the large majority of error locations are found in $H_m^{(d)}$ and $EC^{(d)}$, such an approximation only affects α in Eq. (8) by a small constant factor.

Now, to simulate the circuit $H_m^{(d)}$, we use the fact that $T^\dagger X T = \frac{1}{\sqrt{2}}(X+Z) = H$ and $T^\dagger Z T = \frac{1}{\sqrt{2}}(Z-X) = iYH$. Hence if an X or Z error is input to a T or $T^\dagger$ gate, we pessimistically apply an X or Z error to the output, each with 50% probability. Further, note that an X error propagating through the control qubit of a controlled-Hadamard gate results in a Hadamard error applied to the data (see Fig. 10). Therefore, an $X \otimes X$ error on the first CNOT between the ancillas $|+\rangle$ and $|0\rangle$ in the circuit implementing $H_m^{(d)}$ results in the error $H^{\otimes n}$ (which acts trivially on $|\overline{H}\rangle$) without any flag qubits flagging. However, since the controlled-Hadamard is decomposed as in Fig. 2b, an X error on the control qubit of the controlled-Z gate results in a Z error on the data. Therefore if we propagate $Z^{\otimes n}$ (arising from the $X \otimes X$ error at the CNOT mentioned above) through the T gates as described above, the output will not be a benign error. As such, prior to the application of the T gates, let E_Z be the Z component of the data qubit errors. For instance, if the data qubit errors are $E = Z_1 X_2 Y_3$, then $E_Z = Z_1 Z_3$. The Z component which is propagated through the T gates is chosen to be $E'_Z = \min(\text{wt}(E_Z), \text{wt}(E_Z Z^{\otimes n}))$. This prevents a single fault from causing a logical error without any flag qubits flagging in our simulations.

If all flag qubit and ancilla qubit measurement outcomes in the $(d-1)/2$ applications of the $H_m^{(d)}$ and $EC^{(d)}$ circuits are trivial, the output state is accepted. We define $p_{\text{acc},2}^{(d)}$ to be the probability of acceptance for the second part of the simulation (i.e. the simulation of the $H_m^{(d)}$ and $EC^{(d)}$ circuits) . Hence the total acceptance probability is $p_{\text{acc}}^{(d)} = p_{\text{acc},1}^{(d)} p_{\text{acc},2}^{(d)}$. To determine if the output error of an accepted state is correctable, we perform one round of perfect error correction using the the `Lift` decoder.

The values of $p_L^{(d)}$ and $\langle n_{\text{tot}}^{(d)} \rangle$ for $p \in [10^{-4}, 5\times10^{-4}]$ are given in Table I and were obtained by performing 10^9 Monte-Carlo simulations on AWS clusters. Note that using the $d=5$ version of the protocol in Section III, an $|\overline{H}\rangle$ state can be prepared with logical failure rate 3.6×10^{-8} with using only 68 qubits when $p = 10^{-4}$. Further, one can use the $d=7$ version of the protocol to produce an $|\overline{H}\rangle$ state with logical failure rate 4.9×10^{-10} with only 231 qubits. In [26], magic states with failure rates 4.4×10^{-8} and 9.3×10^{-10} required 810 and 1150 qubits when $p = 10^{-4}$.

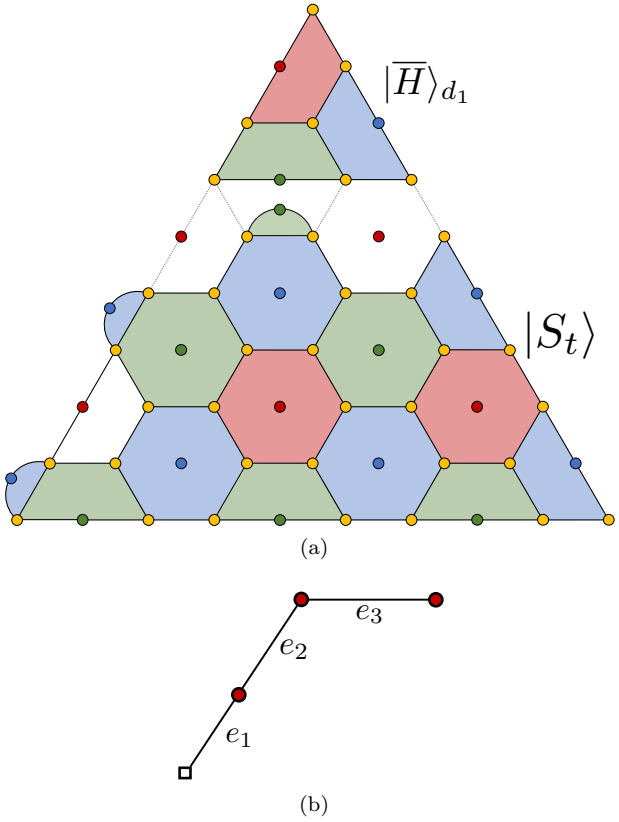

FIG. 11. (a) Illustration for growing an $|\overline{H}\rangle$ state encoded in a $d=3$ triangular color code to one encoded in a $d=7$ triangular color code. A stabilizer state $|S_t\rangle$ is first prepared, and the $d=3$ $|\overline{H}\rangle$ state is prepared following the methods of Section III. One then measures the X and Z-type operators supported on the white plaquettes which anti-commute with the weight-two generators of $\mathcal{S}_{\text{st}}$ resulting in random measurement outcomes. The measurements of all plaquettes are repeated three times to distinguish measurement errors from random measurement outcomes and to correct errors. (b) The matching graph used to implement the weight-two corrections arising from random measurement outcomes of the operators supported on the white plaquettes. As in Fig. 5, each edge corresponds to two qubits supported on a weight-two generator of $\mathcal{S}_{\text{st}}$.

V. PREPARING $|\overline{H}\rangle$ WITH ENCODED STABILIZER OPERATIONS

In Section IV it is shown that using physical Clifford operations, $|\overline{H}\rangle$ states with logical error rates near 10^{-8} and 10^{-10} can be prepared with 68 and 231 qubits. However, for many quantum algorithms, $|\overline{H}\rangle$ states with even lower logical error rates are required. This can be accomplished by encoding all stabilizer operations in a triangular color code since such encoded operations have much lower error rates compared to physical unencoded stabilizer operations. We now describe the implementation of our $|\overline{H}\rangle$ preparation scheme presented in Section III with logical stabilizer operations.

Suppose that in order to prepare an $|\overline{H}\rangle$ state with

$\lvert\overline{H}\rangle_f$	$\lvert\overline{H}\rangle_{d_1}$	p	Color code distance (d_2)	$p_L^{(d_f)}$	$\langle n_f(p, m_{d_f})\rangle$
$d_f = 3$	$d_1 = 7$	10^{-4}	$d_2 = 11$	3.59×10^{-15}	12,143
$d_f = 5$	$d_1 = 5$	10^{-4}	$d_2 = 9$	1.10×10^{-17}	15,447
$d_f = 5$	$d_1 = 5$	2×10^{-4}	$d_2 = 11$	4.01×10^{-16}	26,383
$d_f = 5$	$d_1 = 5$	3×10^{-4}	$d_2 = 15$	6.12×10^{-17}	56,398
$d_f = 7$	$d_1 = 3$	10^{-4}	$d_2 = 7$	5.37×10^{-18}	16,447
$d_f = 7$	$d_1 = 3$	2×10^{-4}	$d_2 = 9$	5.11×10^{-17}	28,498
$d_f = 7$	$d_1 = 3$	3×10^{-4}	$d_2 = 11$	9.87×10^{-17}	44,008
$d_f = 7$	$d_1 = 3$	4×10^{-4}	$d_2 = 13$	5.74×10^{-16}	63,562
$d_f = 7$	$d_1 = 3$	5×10^{-4}	$d_2 = 15$	1.17×10^{-15}	85,575

TABLE II. Various schemes using encoded Clifford gates to obtain $\lvert\overline{H}\rangle_f$ states with logical error rates $p_L^{(d_f)} < 4 \times 10^{-15}$. Here d_2 is color code distance used to encode the logical Clifford gates, d_f is distance used for the $\lvert\overline{H}\rangle$ state preparation scheme of Section III, d_1 is the distance of $\lvert\overline{H}\rangle$ prior to being grown into $\lvert\overline{H}\rangle_{d_2}$ and p is the physical error rate (see Section II B).

$\lvert\overline{H}\rangle_f$	$\lvert\overline{H}\rangle_{d_1}$	p	Surface code distance (d_2)	$p_L^{(d_f)}$	$\langle n_f(p, m_{d_f})\rangle$
$d_f = 7$	$d_1 = 3$	10^{-4}	$d_2 = 5$	5.07×10^{-17}	10,209
$d_f = 7$	$d_1 = 3$	10^{-3}	$d_2 = 11$	8.11×10^{-20}	63,109

TABLE III. Schemes for obtaining an encoded $\lvert\overline{H}\rangle_f$ as in Table II, but with logical Clifford gates encoded in a distance d_2 surface code. Note that the states $\lvert\overline{H}\rangle_{d_2}$ are first encoded in the color code, and lattice surgery is performed to obtain an $\lvert\overline{H}\rangle_{d_2}$ state encoded in the surface code as in [56].

some target logical error rate, we require Clifford gates encoded in a triangular color code of distance d_2. First, $\lvert\overline{H}\rangle_{d_1}$ states used to implement the logical T gates (see Fig. 1) and for injection in the circuit $\lvert\overline{H}\rangle_G$ are prepared using the scheme in Section III (with $d_1 \in \{3, 5, 7\}$ and with physical stabilizer operations). If $d_1 < d_2$, the $\lvert\overline{H}\rangle_{d_1}$ states can be grown into an $\lvert\overline{H}\rangle_{d_2}$ state using a technique analogous to the one illustrated in Fig. 11. The distance d_1 is chosen such that the $\lvert\overline{H}\rangle_{d_1}$ states have smaller logical failure rates compared with those of the encoded Clifford operations. As in Section III A, a stabilizer state $\lvert S_t\rangle$ is prepared, and operators supported on the white plaquettes seperating $\lvert\overline{H}\rangle_{d_1}$ and $\lvert S_t\rangle$ are measured (this step can be viewed as gauge fixing of an underlying subsystem code [57]). Measurements of all operators supported on each plaquette of the distance d_2 triangular color code are repeated d_1 times to correct errors and to distinguish measurement errors from the random outcomes obtained when measuring the white plaquettes.

The states $\lvert\overline{H}\rangle_{d_2}$ (which are prepared as described above) are injected into the circuits to perform the logical T gates, in addition to being injected in the circuit $\lvert\overline{H}\rangle_G$ (see for instance Fig. 5). The final $\lvert\overline{H}\rangle_f$ state used for computation is then prepared repeating the same steps as in Section III with each Clifford gate encoded in the distance d_2 triangular color code.

To compute the overhead for preparing the state $\lvert\overline{H}\rangle_f$, we consider the case where all the $T^\dagger$ gates are simultaneously implemented during the second time step of the $H_m^{(d)}$ circuit. We can thus prepare m_{d_f} $\lvert\overline{H}\rangle_{d_1}$ states which are used for implementing the $T^\dagger$ gates in addition to injecting one of these states into the circuit $\lvert\overline{H}\rangle_G$. The probability that at least $(3d_f+1)/4+1$ $\lvert\overline{H}\rangle_{d_1}$ states pass the verification test is given by

$$P_{A,d_f}(p) = \sum_{k=\frac{3d_f+1}{4}+1}^{m_{d_f}} \binom{m_{d_f}}{k} p_{\text{acc}}^{(d_1)} (1 - p_{\text{acc}}^{(d_1)})^{m_{d_f}-k}, \tag{13}$$

where $p_{\text{acc}}^{(d_1)}$ is the probability of acceptance for preparing the state $\lvert\overline{H}\rangle_{d_1}$. An accepted $\lvert\overline{H}\rangle_{d_1}$ state then grows into an encoded $\lvert\overline{H}\rangle_{d_2}$ state since the Clifford operations are chosen to be encoded in the distance d_2 triangular color code. Since the weight-six stabilizers of the stabilizer state (and all encoded Clifford gates) are obtained from the circuit in Fig. 12, the total number of qubits required for the stabilizer state $\lvert S_t\rangle$ is

$$n_{S_t}(d_1, d_2) = \frac{(3d_2 - 1)^2}{4} - \frac{(3d_1 - 1)^2}{4}, \tag{14}$$

and the number of qubits for each $\lvert\overline{H}\rangle_{d_1}$ state is

$$n_{d_1} = \frac{6{d_1}^2 - 9d_1 + 5}{2}. \tag{15}$$

Lastly, since the qubits in the implementation for preparing $\lvert\overline{H}\rangle_f$ using the protocol of Section III are encoded in the triangular color code with distance d_2, we require an additional

$$n_{\text{add}}(d_1, d_f) = \frac{(3d_2 - 1)^2(6d_f^2 - 9d_f + 6)}{8}, \tag{16}$$

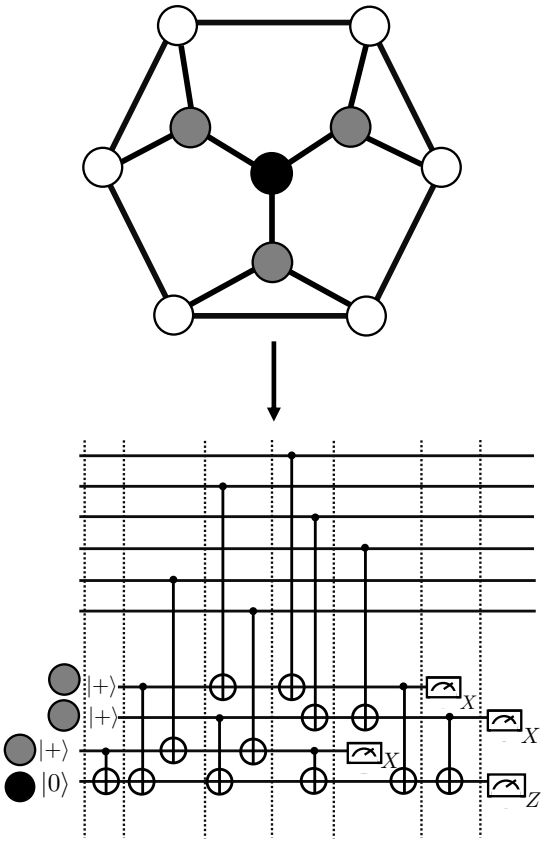

FIG. 12. Weight-six Z-type stabilizer plaquette used in the lattice $\mathcal{L}$ for performing the encoded Clifford operations. The plaquettes used for preparing the stabilizer state $|S_t\rangle$ which is gauge fixed with $|\overline{H}\rangle_{d_1}$ also use the layout shown in this figure. The X-type stabilizer is obtained by inverting the directions of the CNOT gates, swapping $|0\rangle$ with $|+\rangle$ and exchanging the Z-basis measurements with X-basis measurements.

qubits. Hence, the total average number of qubits $\langle n_f \rangle$ required to prepare $|\overline{H}\rangle_f$ is

$$\langle n_f(p, m_{d_f})\rangle = \frac{n_{\text{add}}(d_1, d_f) + m_{d_f}(n_{d_1} + n_{S_t}(d_1, d_2))}{P_{A,d_f}(p) P_{A,H_f}(p)}, \tag{17}$$

where $P_{A,H_f}(p)$ is the acceptance probability for preparing $|\overline{H}\rangle_f$. For a fixed value of p, m_{d_f} is chosen to minimize Eq. (17). Note that we assume that all the qubits used to prepare the m_{d_f} $|\overline{H}\rangle_{d_1}$ magic states can be reused to implement th T gates at the end of the $H_m^{(d)}$ circuit. In doing so, it is assumed that the time scale required to prepare the $|\overline{H}\rangle_{d_2}$ states is less than or equal the time scale required to implemented all the encoded operations prior to applying the T gates at the end of the $H_m^{(d)}$ circuit.

In Table II we provide the average number of qubits required to prepare $|\overline{H}\rangle_f$ states with logical failure rates $p_L^{(d_f)} < 4 \times 10^{-15}$. To obtain such results, we assume that each Clifford gate encoded in the triangular color code fails according to the logical error rate polynomials obtained in [36] (which we call $p_{LC}^{(d_2)}(p)$). Hence, when preparing the stabilizer state $|S_t\rangle$ and for all encoded Clifford operations, the ancilla qubit layout for the weight-six checks are chosen as in Fig. 12 (note that the weight-four checks remain unchanged). Further, the distance d_1 is chosen to be the smallest d_1 which ensures that $|\overline{H}\rangle_{d_1}$ has a lower logical error rate than $p_{LC}^{(d_2)}(p)$. Lastly, due to the low failure rates of the encoded components, to obtain $p_L^{(d_f)}$ we repeat the simulation described in Section IV for physical values of $p > 10^{-3}$, and extrapolate the best fit curves to the regime where $p \in [10^{-4}, 5 \times 10^{-4}]$.

The results obtained in Section II B shows that the least costly scheme to prepare the state $|\overline{H}\rangle_f$ with $p_L^{(d_f)} < 4 \times 10^{-15}$ when $p = 10^{-4}$ is to first prepare the states $|\overline{H}\rangle_{d_1}$ with $d_1 = 7$, and to grow these states to encoded $d_2 = 11$ states. Using distance $d_2 = 11$ encoded stabilizer operations, the final magic state $|\overline{H}\rangle_f$ is prepared using the distance $d_f = 3$ scheme of Section III. On average, the amount of qubits required to prepare such a state is 12,143. To compare with other schemes, in [26], a magic state with a logical error failure rate of 2.4×10^{-15} required 16,400 qubits.

To obtain a state $|\overline{H}\rangle_f$ with $p_L^{(d_f)} \approx 10^{-15}$ when $p = 10^{-3}$ using a small amount of resources requires encoded stabilizer operations with much lower logical failure rates than what is achieved with the triangular color code family. One viable option is to use stabilizer operations encoded in the surface code due to the low error rates that can be achieved when $p = 10^{-3}$ [58]. However, in such a setting, after the states $|\overline{H}\rangle_{d_2}$ have been prepared, they must be teleported to the surface code before they can be injected in the circuit of Fig. 1 and in the circuit implementing $|\overline{H}\rangle_G$. In particular, one can convert the color code encoded state to the surface code using lattice surgery techniques as was done in [56]. In Table III we provide estimates of the qubit overhead for preparing $|\overline{H}\rangle_f$ when the Clifford operations are encoded in the surface code. The cost of first encoding the states $|\overline{H}\rangle_{d_2}$ in the color code and then using extra qubits to convert such states into the surface code is taken into account. However, we assume that the quality of the encoded $|\overline{H}\rangle_{d_2}$ does not change when performing lattice surgery. Although such an omission is optimistic, we verified numerically that when only the T and $T^\dagger$ gate locations are allowed to fail, the protocol of Section III produces $|\overline{H}\rangle_f$ states with logical error rates two to four orders of magnitude (depending on the value of p) less than when all Clifford operations fail according to the noise model described in Section II B. As such, the simulation provides evidence that the logical error rates obtained in Table III are good estimates of the error rates that would be obtained when considering errors introduced when performing lattice surgery to obtain surface code encoded $|\overline{H}\rangle_{d_2}$ states.

Instead of performing lattice surgery to convert a color

code encoded $|\overline{H}\rangle_{d_2}$ state to one encoded in the surface code, another option would be to initially prepare an encoded $|\overline{H}\rangle_{d_2}$ state in a small distance surface code using some other method, such as a magic state distillation protocol. The $|\overline{H}\rangle_{d_2}$ states would then be injected in the T gate circuits of Fig. 1 in addition to the $|\overline{H}\rangle_G$ circuit (Section III A) in order to prepare an $|\overline{H}\rangle_f$ state using the methods presented in Section III. To obtain comparable logical failure rates to the ones shown in Table II at $p = 10^{-3}$, from [58], the surface code distance d_2 would need to be $d_2 = 15$ if the $d_f = 3$ scheme was chosen, $d_2 = 13$ if the $d_f = 5$ scheme was chosen and $d_2 = 11$ if the $d_f = 7$ scheme were chosen. A careful analysis of the overhead would require choosing the appropriate magic state distillation protocol (or some other scheme which uses fault-tolerant circuits to prepare encoded magic states) and therefore such an analysis is left for future work.

VI. CONCLUSION AND OUTLOOK

In this work we showed how to prepare an $|H\rangle$-type magic state in a fault-tolerant way using a two-dimensional color code architecture requiring only nearest-neighbor interactions. The proposed architecture can be used to both measure local stabilizers of the color code in addition to a global operator, without the need for changing the qubit layout. Such an architecture was made possible with the use of flag qubits, in addition to a new concept which we call redundant ancilla encoding. Estimating the performance of our scheme, we showed that when $p = 10^{-4}$, only 68 and 231 qubits are required to prepare an encoded $|H\rangle$ state with logical error rates 3.6×10^{-8} and 4.9×10^{-10} respectively. In addition, we also showed how our scheme can be used with encoded stabilizer operations to achieve significantly lower logical failure rates, both in the regime where $p = 10^{-4}$ and $p = 10^{-3}$. We stress that our results were obtained by considering a full circuit-level depolarizing noise model, where all stabilizer operations could fail.

The underlying codes that are used for our work belong to the triangular color code family. One avenue of exploration would be to consider the 4.8.8 color code family for potentially better performance. In addition, the color codes used to encode the Clifford operations used two and three ancillas for the weight-four and weight-six stabilizers respectively. Using similar edge weight renormalization schemes to those used in [36], it could be possible to use fewer ancillas for each stabilizer while maintaining the full effective code distance of the `Lift` decoder. Due to the smaller number of fault locations and reduced ancilla requirements, such an implementation could potentially significantly reduce the overhead for preparing $|H\rangle$ states.

When considering the implementation of our scheme with encoded Clifford operations using the surface code, the $d_f = 7$ version of our scheme was optimal for both $p = 10^{-4}$ and $p = 10^{-3}$. A clear direction of future work would be to find a v-flag circuit (with $v \geq 4$) allowing a fault-tolerant implementation of a $d_f \geq 9$ scheme. Such a scheme could potentially further reduce the overhead for preparing $|H\rangle$ states with very low error rates.

The schemes considered in this work to prepare $|H\rangle$ states are error detection schemes. In particular, for $p = 10^{-3}$ and $d_f > 3$, the acceptance probability for preparing an $|H\rangle$ state is very low (for instance, only 12% when $d_f = 5$). One way to improve the acceptance probability could be to use qubits encoded in a bosonic code (such as a GKP code [59]) and concatenate such qubits with the color code (the GKP code concatenated with the surface code was considered in [60, 61] for quantum memories). By using bosonic qubits, repeated rounds of error correction at the bosonic level prior to measuring the logical Hadamard operator and stabilizers of the color code could be performed to reduce some of the errors afflicting the data and ancilla qubits. Another possibility would be to develop an error correction scheme for preparing an $|H\rangle$ state which applies directly to the color code family. Such a scheme would have higher logical error rates compared to an error detection scheme, and the scheduling of the controlled-Hadamard gates would have to be considered more carefully. However, since an error correction scheme would not require any post selection, there could be an interval of physical error rates where it achieved better performance compared to the error detection scheme considered in this work.

ACKNOWLEDGMENTS

C.C. acknowledges Yihe Tang and Milan Cvitkovic for their help in setting up the computing resources with the AWS clusters which were used for performing all the numerical simulations in this work.

Appendix A: Non fault-tolerant $|H\rangle$ state preparation scheme

Appendix B: Repeating the Hadamard measurement and EC circuits

In this section we show that in order for the magic state preparation protocol of Section III to be fault-tolerant, the $H_m^{(d)}$ and $EC^{(d)}$ circuits both need to be repeated a minimum of $(d-1)/2$ times. In what follows, we say that a state preparation protocol is t-fault-tolerant if the following two conditions are satisfied (see for instance [13, 62]):

Definition 2. *Fault-tolerant state preparation*

For $t = (d-1)/2$, a state-preparation protocol using a distance-d stabilizer code C is t-fault-tolerant if the following two conditions are satisfied:

1. *If there are s faults during the state-preparation protocol with $s \leq t$, the resulting state differs from a codeword by an error of at most weight s.*

2. *If there are s faults during the state-preparation protocol with $s \leq t$, then ideally decoding the output state results in the same state that would be obtained from the fault-free state-preparation scheme.*

In what follows the code C belongs to the triangular color code family. Further, since the $H_m^{(d)}$ circuits are valid for $d \in \{3, 5, 7\}$, the following arguments apply for code distances of the triangular color code that are no greater than seven.

We have already verified numerically that the $H_m^{(d)}$ and $EC^{(d)}$ circuits are t-flag circuits (with $t = (d-1)/2$). Hence if there are $s \leq t$ faults in the $H_m^{(d)}$ and $EC^{(d)}$ circuits resulting in an error E with $\mathrm{wt}(E) > s$, at least one flag qubit will flag and the protocol aborts. Therefore, we first focus on input errors to the $H_m^{(d)}$ circuits arising from faults which occur in the $|\overline{H}\rangle_G$ circuit.

Suppose s_1 faults occur in the $|\overline{H}\rangle_G$ circuit and s_2 faults occur in the $H_m^{(d)}$ circuit, where $s_1 + s_2 \leq t$. In general, the input to the $H_m^{(d)}$ circuit has the form

$$E_{\text{in}}^{(1)} = E'\overline{E}. \tag{B1}$$

In Eq. (B1), $\overline{E} \in \{I, \overline{X}, \overline{Y}, \overline{Z}\}$ is the logical identity or a logical operator of the distance d triangular color code. The operator E' is either the identity, or has a non-trivial syndrome (i.e. $s(E') \neq \mathbf{0}$ where $s(E)$ is the error syndrome of the error E obtained by measuring all stabilizer generators of the distance d triangular color code). Now, from the above, we can assume that the s_2 faults in the $H_m^{(d)}$ circuits do not cause any flag qubits to flag. We can also assume that $E' = I$ since otherwise E' will be detected by the $EC^{(d)}$ circuit. If $s_2 = 0$, then a $+1$ measurement outcome of the $H_m^{(d)}$ circuit always results in an output state with no logical error (see Appendix C). Hence consider the worst case, where $s_1 = 1$ (with $\overline{E} \neq I$ in Eq. (B1)) and $s_2 = t - 1 = (d-1)/2 - 1$, where each fault in $H_m^{(d)}$ corresponds to a measurement error such that all Hadamard measurement outcomes are $+1$.

Now suppose the $H_m^{(d)}$ circuit is applied $(d-1)/2$ times. Since $s_2 = (d-3)/2$, at least one of the $H_m^{(d)}$ circuits will not be afflicted by a measurement error. Consequently, the measurement outcome of the fault-free $H_m^{(d)}$ circuit is either -1 (in which case the protocol is aborted) or $+1$ (in which case the output state is not afflicted by a logical fault). This conclusion could not be guaranteed if the $H_m^{(d)}$ circuit was applied less than $(d-1)/2$ times.

Lastly, consider the case where s_1 faults occurred in the $|\overline{H}\rangle_G$ circuit, s_2 faults occurred in the $H_m^{(d)}$ circuits and s_3 faults occurred in the $EC^{(d)}$ circuits with $s_1 + s_2 + s_3 \leq t$. Further, assume that all measurement outcomes in the $H_m^{(d)}$ circuits were $+1$. A general input error to the first $EC^{(d)}$ circuit can be written as

$$E_{\text{in}}^{(2)} = c \sum_i \sum_{j \in \{I,X,Y,Z\}} E_i \overline{E}_j, \tag{B2}$$

where c is a normalization coefficient and $\overline{E}_I$ acts trivially on the encoded state. Note that from the previous arguments, $E_{\text{in}}^{(2)}$ cannot be a pure logical operator (i.e. $s(E_{\text{in}}^{(2)}) = \mathbf{0}$) since otherwise at least one of the measurement outcomes of the $H_m^{(d)}$ circuits would be non-trivial.

Again, we can imagine the worst case scenario where a single fault prior to the $EC^{(d)}$ circuits results in an input error $E_{\text{in}}^{(2)}$ with $s(E_{\text{in}}^{(2)}) = \mathbf{0}$ (so that $s_1 + s_2 = 1$) and $s_3 = t - 1$ measurement errors occur in the $EC^{(d)}$ circuits resulting in trivial measurement outcomes of all stabilizers in each $EC^{(d)}$ circuit afflicted by a fault. Therefore, if the $EC^{(d)}$ circuit is repeated $(d-1)/2$ times, then at least one of the circuits will be fault-free and the error $E_{\text{in}}^{(2)}$ will be detected, in which case the protocol will be aborted.

Since the $H_m^{(d)}$ and $EC^{(d)}$ circuits are t-flag circuits and from the arguments presented in this section, if there are a total $s \leq t$ faults during our $|H\rangle$ state preparation protocol, then the output state has the form $|\psi_{\text{out}}\rangle = E'|\overline{H}\rangle$ with $\mathrm{wt}(E') \leq s$. Hence both conditions in Definition 2 are trivially satisfied.

Appendix C: Fault-free measurement outcomes of the $H_m^{(d)}$ circuits for arbitrary input errors

[1] Bryan Eastin and Emanuel Knill. Restrictions on transversal encoded quantum gate sets. *Phys. Rev. Lett.*, 102:110502, Mar 2009. doi: 10.1103/PhysRevLett.102.110502. URL https://link.aps.org/doi/10.1103/PhysRevLett.102.110502.

[2] Emanuel Knill, Raymond Laflamme, and Wojciech H. Zurek. Threshold accuracy for quantum computation. *arXiv: quant-ph/9610011*, 1996.

[3] Adam Paetznick and Ben W. Reichardt. Universal fault-tolerant quantum computation with only transversal gates and error correction. *Phys. Rev. Lett.*, 111:090505, Aug 2013. doi:10.1103/PhysRevLett.111.090505. URL https://link.aps.org/doi/10.1103/PhysRevLett.111.090505.

[4] Tomas Jochym-O'Connor and Raymond Laflamme. Using concatenated quantum codes for universal fault-tolerant quantum gates. *Phys. Rev. Lett.*, 112:010505, 2014. doi:10.1103/PhysRevLett.112.010505. URL

http://link.aps.org/doi/10.1103/PhysRevLett.112.010505.

[5] Jonas T. Anderson, Guillaume Duclos-Cianci, and David Poulin. *Phys. Rev. Lett.*, 113:080501, Aug 2014. doi: 10.1103/PhysRevLett.113.080501. URL https://link.aps.org/doi/10.1103/PhysRevLett.113.080501.

[6] Héctor Bombín. Gauge color codes: optimal transversal gates and gauge fixing in topological stabilizer codes. *New J. Phys.*, 17(8):083002, 2015. URL https://iopscience.iop.org/article/10.1088/1367-2630/17/8/083002/meta.

[7] Sergey Bravyi and Andrew Cross. Doubled Color Codes. *arXiv e-prints*, art. arXiv:1509.03239, Sep 2015. URL https://arxiv.org/abs/1509.03239.

[8] Tomas Jochym-O'Connor and Stephen D. Bartlett. Stacked codes: Universal fault-tolerant quantum computation in a two-dimensional layout. *Phys. Rev. A*, 93:022323, 2016. doi:10.1103/PhysRevA.93.022323. URL http://link.aps.org/doi/10.1103/PhysRevA.93.022323.

[9] Theodore J. Yoder, Ryuji Takagi, and Isaac L. Chuang. Universal fault-tolerant gates on concatenated stabilizer codes. *Phys. Rev. X*, 6:031039, Sep 2016. doi: 10.1103/PhysRevX.6.031039. URL https://link.aps.org/doi/10.1103/PhysRevX.6.031039.

[10] Christopher Chamberland, Tomas Jochym-O'Connor, and Raymond Laflamme. Thresholds for universal concatenated quantum codes. *Phys. Rev. Lett.*, 117:010501, Jun 2016. doi:10.1103/PhysRevLett.117.010501. URL https://link.aps.org/doi/10.1103/PhysRevLett.117.010501.

[11] Christopher Chamberland, Tomas Jochym-O'Connor, and Raymond Laflamme. Overhead analysis of universal concatenated quantum codes. *Phys. Rev. A*, 95:022313, Feb 2017. doi:10.1103/PhysRevA.95.022313. URL https://link.aps.org/doi/10.1103/PhysRevA.95.022313.

[12] Christopher Chamberland and Tomas Jochym-OConnor. Error suppression via complementary gauge choices in reed-muller codes. *Quantum Science and Technology*, 2(3):035008, 2017. URL http://stacks.iop.org/2058-9565/2/i=3/a=035008.

[13] Christopher Chamberland and Andrew W. Cross. Fault-tolerant magic state preparation with flag qubits. *Quantum*, 3:143, May 2019. ISSN 2521-327X. doi: 10.22331/q-2019-05-20-143. URL https://doi.org/10.22331/q-2019-05-20-143.

[14] Tomas Jochym-O'Connor. Fault-tolerant gates via homological product codes. *Quantum*, 3:120, February 2019. ISSN 2521-327X. doi:10.22331/q-2019-02-04-120. URL https://doi.org/10.22331/q-2019-02-04-120.

[15] Ali Lavasani, Guanyu Zhu, and Maissam Barkeshli. Universal logical gates with constant overhead: instantaneous Dehn twists for hyperbolic quantum codes. *Quantum*, 3:180, August 2019. ISSN 2521-327X. doi: 10.22331/q-2019-08-26-180. URL https://doi.org/10.22331/q-2019-08-26-180.

[16] Sergey Bravyi and Alexei Kitaev. Universal quantum computation with ideal clifford gates and noisy ancillas. *Phys. Rev. A*, 71:022316, Feb 2005. doi: 10.1103/PhysRevA.71.022316. URL https://link.aps.org/doi/10.1103/PhysRevA.71.022316.

[17] Ben W. Reichardt. Quantum universality from magic states distillation applied to css codes. *Quantum Information Processing*, 4(3):251–264, Aug 2005. ISSN 1573-1332. doi:10.1007/s11128-005-7654-8. URL https://doi.org/10.1007/s11128-005-7654-8.

[18] Adam M. Meier, Bryan Eastin, and Emanuel Knill. Magic-state distillation with the four-qubit code. *Quantum Info. Comput.*, 13(3-4):0195–0209, 2013.

[19] Sergey Bravyi and Jeongwan Haah. Magic-state distillation with low overhead. *Phys. Rev. A*, 86:052329, Nov 2012. doi:10.1103/PhysRevA.86.052329. URL https://link.aps.org/doi/10.1103/PhysRevA.86.052329.

[20] Austin G. Fowler, Simon J. Devitt, and Cody Jones. Surface code implementation of block code state distillation. *Scientific Reports*, (3):1939, 2013. doi: 10.1038/srep01939.

[21] Joe O'Gorman and Earl T. Campbell. Quantum computation with realistic magic-state factories. *Phys. Rev. A*, 95:032338, Mar 2017. doi: 10.1103/PhysRevA.95.032338. URL https://link.aps.org/doi/10.1103/PhysRevA.95.032338.

[22] Jeongwan Haah, Matthew B. Hastings, D. Poulin, and D. Wecker. Magic state distillation with low space overhead and optimal asymptotic input count. *Quantum*, 1:31, October 2017. ISSN 2521-327X. doi: 10.22331/q-2017-10-03-31. URL https://doi.org/10.22331/q-2017-10-03-31.

[23] Jeongwan Haah, Matthew B. Hastings, David Poulin, and Dave Wecker. Magic state distillation at intermediate size. *Quantum Info. Comput.*, 18(1):97–165, 2018. ISSN 0114-0140.

[24] Matthew B. Hastings and Jeongwan Haah. Distillation with sublogarithmic overhead. *Phys. Rev. Lett.*, 120:050504, Jan 2018. doi:10.1103/PhysRevLett.120.050504. URL https://link.aps.org/doi/10.1103/PhysRevLett.120.050504.

[25] Jeongwan Haah and Matthew B. Hastings. Codes and Protocols for Distilling T, controlled-S, and Toffoli Gates. *Quantum*, 2:71, June 2018. ISSN 2521-327X. doi: 10.22331/q-2018-06-07-71. URL https://doi.org/10.22331/q-2018-06-07-71.

[26] Daniel Litinski. Magic State Distillation: Not as Costly as You Think. *Quantum*, 3:205, December 2019. ISSN 2521-327X. doi:10.22331/q-2019-12-02-205. URL https://doi.org/10.22331/q-2019-12-02-205.

[27] Theodore J. Yoder and Isaac H. Kim. The surface code with a twist. *Quantum*, 1:2, April 2017. ISSN 2521-327X. doi:10.22331/q-2017-04-25-2. URL https://doi.org/10.22331/q-2017-04-25-2.

[28] Rui Chao and Ben W. Reichardt. Quantum error correction with only two extra qubits. *Phys. Rev. Lett.*, 121:050502, Aug 2018. doi: 10.1103/PhysRevLett.121.050502. URL https://link.aps.org/doi/10.1103/PhysRevLett.121.050502.

[29] Rui Chao and Ben W. Reichardt. Fault-tolerant quantum computation with few qubits. *npj Quantum Information*, 4(1):42, 2018. doi:10.1038/s41534-018-0085-z. URL https://doi.org/10.1038/s41534-018-0085-z.

[30] Christopher Chamberland and Michael E. Beverland. Flag fault-tolerant error correction with arbitrary distance codes. *Quantum*, 2:53, February 2018. ISSN 2521-327X. doi:10.22331/q-2018-02-08-53. URL https://doi.org/10.22331/q-2018-02-08-53.

[31] Theerapat Tansuwannont, Christopher Chamberland, and Debbie Leung. Flag fault-tolerant error correction, measurement, and quantum computation for

cyclic calderbank-shor-steane codes. *Phys. Rev. A*, 101: 012342, Jan 2020. doi:10.1103/PhysRevA.101.012342. URL https://link.aps.org/doi/10.1103/PhysRevA.101.012342.

[32] Ben W. Reichardt. Fault-tolerant quantum error correction for steane's seven-qubit color code with few or no extra qubits. *arXiv:quant-ph/1804.06995*, 2018. URL https://arxiv.org/abs/1804.06995.

[33] Yunong Shi, Christopher Chamberland, and Andrew Cross. Fault-tolerant preparation of approximate GKP states. *New Journal of Physics*, 21(9):093007, sep 2019. doi:10.1088/1367-2630/ab3a62. URL https://doi.org/10.1088%2F1367-2630%2Fab3a62.

[34] Christopher Chamberland, Guanyu Zhu, Theodore J. Yoder, Jared B. Hertzberg, and Andrew W. Cross. Topological and subsystem codes on low-degree graphs with flag qubits. *Phys. Rev. X*, 10:011022, Jan 2020. doi: 10.1103/PhysRevX.10.011022. URL https://link.aps.org/doi/10.1103/PhysRevX.10.011022.

[35] Rui Chao and Ben W. Reichardt. Flag fault-tolerant error correction for any stabilizer code. *arXiv e-prints*, art. arXiv:1912.09549, Dec 2019.

[36] Christopher Chamberland, Aleksander Kubica, Theodore J Yoder, and Guanyu Zhu. Triangular color codes on trivalent graphs with flag qubits. *New Journal of Physics*, 22(2):023019, feb 2020. doi:10.1088/1367-2630/ab68fd. URL https://doi.org/10.1088%2F1367-2630%2Fab68fd.

[37] H. Bombin and M. A. Martin-Delgado. Topological quantum distillation. *Phys. Rev. Lett.*, 97:180501, Oct 2006. doi:10.1103/PhysRevLett.97.180501. URL https://link.aps.org/doi/10.1103/PhysRevLett.97.180501.

[38] Aleksander Kubica and Michael E. Beverland. Universal transversal gates with color codes: A simplified approach. *Phys. Rev. A*, 91:032330, 2015. doi: 10.1103/PhysRevA.91.032330. URL http://link.aps.org/doi/10.1103/PhysRevA.91.032330.

[39] Aleksander Kubica. *The ABCs of the color code: A study of topological quantum codes as toy models for fault-tolerant quantum computation and quantum phases of matter*. PhD thesis, 2018. URL https://thesis.library.caltech.edu/10955/.

[40] Aleksander Kubica and Nicolas Delfosse. Efficient color code decoders in $d \geq 2$ dimensions from toric code decoders. *arXiv e-prints*, art. arXiv:1905.07393, May 2019. URL https://arxiv.org/abs/1905.07393.

[41] Alexei Y. Kitaev. Quantum computations: algorithms and error correction. *Russian Mathematical Surveys*, 52 (6):1191–1249, 1997.

[42] Christopher M. Dawson and Michael Nielsen. The solovay-kitaev algorithm. *Quant. Inf. Comput.*, 6:81–95, 2006.

[43] Austin G. Fowler, Matteo Mariantoni, John M. Martinis, and Andrew N. Cleland. Surface codes: Towards practical large-scale quantum computation. *Phys. Rev. A*, 86:032324, Sep 2012. doi:10.1103/PhysRevA.86.032324. URL https://link.aps.org/doi/10.1103/PhysRevA.86.032324.

[44] Ian D. Kivlichan, Craig Gidney, Dominic W. Berry, Nathan Wiebe, Jarrod McClean, Wei Sun, Zhang Jiang, Nicholas Rubin, Austin Fowler, Alán Aspuru-Guzik, Hartmut Neven, and Ryan Babbush. Improved Fault-Tolerant Quantum Simulation of Condensed-Phase Correlated Electrons via Trotterization. *arXiv e-prints*, art. arXiv:1902.10673, Feb 2019. URL https://arxiv.org/abs/1902.10673.

[45] Craig Gidney and Martin Ekerå. How to factor 2048 bit RSA integers in 8 hours using 20 million noisy qubits. *arXiv e-prints*, art. arXiv:1905.09749, May 2019. URL https://arxiv.org/abs/1905.09749.

[46] Panos Aliferis, Daniel Gottesman, and John Preskill. Quantum accuracy threshold for concatenated distance-3 codes. *Quantum Info. Comput.*, 6(2):97–165, March 2006. ISSN 1533-7146. URL http://dl.acm.org/citation.cfm?id=2011665.2011666.

[47] Emanuel Knill. Quantum computing with realistically noisy devices. *Nature*, 434(7029):39–44, 2005. doi: 10.1038/nature03350. URL https://www.nature.com/articles/nature03350.

[48] Barbara M. Terhal. Quantum error correction for quantum memories. *Rev. Mod. Phys.*, 87:307–346, Apr 2015. doi:10.1103/RevModPhys.87.307. URL https://link.aps.org/doi/10.1103/RevModPhys.87.307.

[49] David P. DiVincenzo and Panos Aliferis. Effective fault-tolerant quantum computation with slow measurements. *Phys. Rev. Lett.*, 98:020501, Jan 2007. doi: 10.1103/PhysRevLett.98.020501. URL https://link.aps.org/doi/10.1103/PhysRevLett.98.020501.

[50] Christopher Chamberland, Pavithran Iyer, and David Poulin. Fault-Tolerant Quantum Computing in the Pauli or Clifford Frame with Slow Error Diagnostics. *Quantum*, 2:43, January 2018. ISSN 2521-327X. doi: 10.22331/q-2018-01-04-43. URL https://doi.org/10.22331/q-2018-01-04-43.

[51] Jack Edmonds. Paths, trees, and flowers. *Canadian Journal of mathematics*, 17 (3):449–467, 1965. doi:10.4153/CJM-1965-045-4. URL https://www.cambridge.org/core/journals/canadian-journal-of-mathematics/article/paths-trees-and-flowers/08B492B72322C4130AE800C0610E0E21.

[52] Peter W. Shor. Fault-tolerant quantum computation. *Proceedings., 37th Annual Symposium on Foundations of Computer Science*, pages 56–65, 1996. URL http://dl.acm.org/citation.cfm?id=874062.875509.

[53] David P. DiVincenzo and Peter W. Shor. Fault-tolerant error correction with efficient quantum codes. *Phys. Rev. Lett.*, 77:3260–3263, Oct 1996. doi: 10.1103/PhysRevLett.77.3260. URL https://link.aps.org/doi/10.1103/PhysRevLett.77.3260.

[54] Daniel Gottesman. The Heisenberg representation of quantum computers. *Proceedings, XXII International Colloquium on Group Theoretical Methods in Physics*, pages 32–43, 1999.

[55] Scott Aaronson and Daniel Gottesman. Improved simulation of stabilizer circuits. *Phys. Rev. A*, 70:052328, Nov 2004. doi:10.1103/PhysRevA.70.052328. URL https://link.aps.org/doi/10.1103/PhysRevA.70.052328.

[56] Hendrik Poulsen Nautrup, Nicolai Friis, and Hans J. Briegel. Fault-tolerant interface between quantum memories and quantum processors. *Nature Communications*, 8: 1321, NOV 2017. doi:10.1038/s41467-017-01418-2. URL https://doi.org/10.1038/s41467-017-01418-2.

[57] Christophe Vuillot, Lingling Lao, Ben Criger, Carmen García Almudéver, Koen Bertels, and Barbara M Terhal. Code deformation and lattice surgery are gauge fixing. *New Journal of Physics*, 21(3):033028, mar 2019. doi:10.1088/1367-2630/ab0199. URL https://doi.org/

10.1088%2F1367-2630%2Fab0199.

[58] Austin G. Fowler, Adam C. Whiteside, Angus L. McInnes, and Alimohammad Rabbani. Topological code autotune. *Phys. Rev. X*, 2:041003, Oct 2012. doi: 10.1103/PhysRevX.2.041003. URL https://link.aps.org/doi/10.1103/PhysRevX.2.041003.

[59] Daniel Gottesman, Alexei Kitaev, and John Preskill. Encoding a qubit in an oscillator. *Phys. Rev. A*, 64: 012310, Jun 2001. doi:10.1103/PhysRevA.64.012310. URL https://link.aps.org/doi/10.1103/PhysRevA.64.012310.

[60] Christophe Vuillot, Hamed Asasi, Yang Wang, Leonid P. Pryadko, and Barbara M. Terhal. Quantum error correction with the toric gottesman-kitaev-preskill code. *Phys. Rev. A*, 99:032344, Mar 2019. doi: 10.1103/PhysRevA.99.032344. URL https://link.aps.org/doi/10.1103/PhysRevA.99.032344.

[61] Kyungjoo Noh and Christopher Chamberland. Fault-tolerant bosonic quantum error correction with the surface–gottesman-kitaev-preskill code. *Phys. Rev. A*, 101:012316, Jan 2020. doi:10.1103/PhysRevA.101.012316. URL https://link.aps.org/doi/10.1103/PhysRevA.101.012316.

[62] Daniel Gottesman. An introduction to quantum error correction and fault-tolerant quantum computation. *Proceedings of Symposia in Applied Mathematics*, 68:13–58, 2010. URL https://arxiv.org/abs/0904.2557.